

LOMS.cz: A computational platform for high-throughput Classical and Combinatorial Judd-Ofelt analysis and rare-earth spectroscopy

Jan Hrabovsky^{1,*,+}, Petr Varak^{2,3,+}, and Robin Krystufek^{4,5,+}

¹Charles University, Faculty of Mathematics and Physics, Ke Karlovu 5, 121 16 Prague, Czech Republic

²Department of Inorganic Chemistry, Faculty of Chemical Technology, University of Chemistry and Technology, Prague, Technicka 5, 166 28 Prague, Czech Republic

³Institute of Photonics and Electronics of the Czech Academy of Sciences, Chaberska 1014/57, 182 00 Prague Czech Republic

⁴Institute of Organic Chemistry and Biochemistry of the Czech Academy of Sciences, Flemingovo n. 2, Prague 6 16610, Czech Republic

⁵Department of Physical and Macromolecular Chemistry, Faculty of Science, Charles University Hlavova 8, Prague 2 12843, Czech Republic

*jan.hrabovsky@mff.cuni.cz

+these authors contributed equally to this work

ABSTRACT

We present LOMS.cz (Luminescence, Optical and Magneto-optical Software), an open-source computational platform that addresses the long-standing challenge of standardizing Judd-Ofelt (JO) calculations in rare-earth spectroscopy. Despite JO theory's six-decade history as the fundamental framework for understanding $4f \leftrightarrow 4f$ transitions, the field lacks standardized computational methodologies for precise and reproducible parameter determination. LOMS integrates three key innovations: (1) automated computation of JO parameters, transition probabilities, branching ratios, and theoretical radiative lifetimes, (2) a dynamically expanding database of experimentally validated parameters enabling direct comparison between computed and empirical results, and (3) a novel Combinatorial JO (C-JO) analysis algorithm that systematically identifies optimal absorption band combinations to ensure reliable parameter extraction. As a proof-of-concept, we demonstrate how this computational framework enables rapid screening of spectroscopic parameters, allowing researchers to predict optical properties with enhanced reliability. By combining automated analysis with experimental validation through its integrated database, LOMS establishes a standardized platform for accelerating the discovery and optimization of rare-earth-based photonic and optoelectronic materials.

The computational design and characterization of rare-earth (RE) materials represents a critical challenge in materials science, particularly given their essential role in modern technology. RE elements, especially their trivalent ions, exhibit unique electronic, magnetic, and spectroscopic properties that make them indispensable in various high-tech applications¹⁻⁴. Within the industrial sector, RE ions are essential components in the manufacturing process of strong permanent magnets, which are used in electric cars, imaging devices such as the screen of smartphones/computers or as catalysts in chemical reactions^{1,5-7}. Furthermore, their luminescent properties are used for medical imaging as diagnostic tools, enhancing the capabilities of modern healthcare technologies^{1,2,8,9}. The global market for RE-based products, reaching nearly \$2 trillion by 2012 (approximately 5% of global GDP), underscores their technological significance^{10,11}.

A major challenge in RE materials research is the standardized analysis of their optical properties. Despite extensive experimental knowledge of the spectroscopic properties of rare-earth ions, the correct mechanism of the strong intra $4f \leftrightarrow 4f$ electronic transitions was only understood around the mid-20th century thanks to the advances in Racah's algebra and the enhanced computational capabilities brought by advancements in computer technology^{2,12,13}. Building on these previous accomplishments, B.R. Judd¹⁴ and G.S. Ofelt¹⁵ independently introduced a theory in 1962 that describes the spectroscopic properties of rare-earth ions in various materials. These studies thus established the foundation for what later became known as the Judd-Ofelt (JO) theory, the first quantum-mechanical explanation of the electric-dipole induced $4f \leftrightarrow 4f$ transition intensities in RE ions through the set of three JO parameters $\Omega_i (i = 2, 4, 6)$. These parameters enable the prediction of spectroscopic properties crucial for designing and optimizing photonic materials and devices, including transition probabilities

35 $A(J', J)$, branching ratios $\beta(J', J)$, and theoretical luminescence radiative lifetimes, τ_r^{JO} . The exponential growth in JO theory
 36 applications, evidenced by over 19,000 publications by mid-2024 (see Fig. 1), reflects three primary research directions: (1)
 37 theoretical advancement of JO parametrization methods^{2,12,13,16-18}, (2) experimental characterization across diverse material
 38 systems¹⁹, and (3) integration of JO analysis into broader materials design strategies^{12,13,20,21}. It should be noted that the last
 39 two categories make up the majority of published works and primarily focus on the practical implementation of JO theory
 40 rather than its theoretical understanding. However, a significant need remains for standardized experimental understanding
 41 and accessible computational tools to facilitate the practical implementation of JO theory and the reliable extraction of JO
 42 parameters. These include the complexity of selecting appropriate absorption bands for analysis, the challenge of ensuring
 43 reproducible parameter extraction, and the lack of systematic comparison between theoretical predictions and experimental
 44 results. To address these challenges, we developed Luminescence, Optics and Magneto-optics Software (LOMS), an open-source
 45 computational platform that automates and standardizes JO analysis. Our implementation of newly introduced Combinatorial
 46 JO (C-JO) analysis represents a significant advance in computational methodology, enabling systematic identification of optimal
 47 absorption band combinations for reliable parameter extraction. The LOMS.cz platform further introduces the first dynamic,
 48 automatically organized repository of JO parameters, facilitating direct comparison between computed and experimental results.
 49 Given a set of absorption spectra, the platform can fully automate the entire computational workflow, from initial parameter
 50 calculation through property prediction. As demonstrated below, LOMS can systematically analyze spectroscopic parameters
 51 and predict optical properties while providing detailed uncertainty quantification through its comprehensive analysis approach.
 52 The platform enables researchers to efficiently evaluate materials properties and optimize RE-doped systems for specific
 53 applications, accelerating the development of next-generation photonic and optoelectronic materials through standardized
 54 computational analysis.

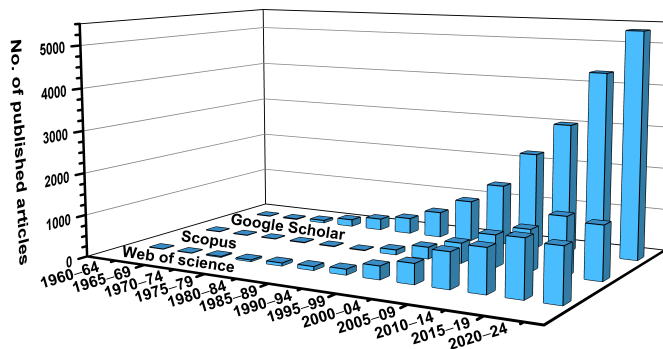


Figure 1. Tracking of "Judd-Ofelt" expression within Google Scholar, Scopus and Web of sciences (WOS) scientific databases in 5-year intervals by July 2024.

55 Results

56 Method outline: Judd-Ofelt theory and Rare-earth ions

57 To introduce JO theory and its implications, it is first necessary to define basic concepts related to the physics of rare-earth
 58 elements/ions, derivation of spectroscopic terms for RE³⁺ ground states as well as to know the position of other multiplets in
 59 energy diagram and other aspects required for in-depth spectroscopic description of solid. However, this section does not aim
 60 to provide an exhaustive mathematical treatment of JO theory and quantum mechanical descriptions, which are extensively
 61 detailed in original studies by Judd¹⁴ and Ofelt¹⁵ or comprehensive works by Hehlen¹² and Walsh². Instead, the primary
 62 goal is to present JO theory from an experimental perspective and introduce it to the broader scientific community. Presented
 63 outcomes are then introduced in the form of the interactive free-to-use computational online tool (www.LOMS.cz/jo) designed
 64 for calculating classical and combinatorial JO analysis and related parameters, facilitating accessibility and practical application
 65 of the theory. The calculated results can then be directly compared in the newly established JO parameter database on the same
 66 web platform (www.LOMS.cz/jo-database).

67 Rare-earth ions: spectroscopic properties and application

68 The Rare-earth (RE) elements consist of seventeen chemical elements in the periodic table, including fifteen lanthanides (La, 69 Ce, Pr, Nd, Pm, Sm, Eu, Gd, Tb, Dy, Ho, Er, Tm, Yb, Lu) along with Sc and Y. While rare-earth ions typically form trivalent cations, exceptions exist where divalent (Nd²⁺, Sm²⁺, Eu²⁺, Dy²⁺, Tm²⁺, Yb²⁺) and quadrivalent (Ce⁴⁺, Pr⁴⁺, Tb⁴⁺, D⁴⁺) 70 cations can also be formed. Rare-earth ions are widely used in electronics and in the production of magnets, catalysts, and 71 photonics materials, with trivalent (RE³⁺) cations being the most commonly utilized for these applications^{1,4-7}. For this reason, 72 the main focus will be on trivalent rare-earth cations with at least partially occupied 4f electron orbital and charge configuration 73 of [Xe] 4f¹⁻¹³. Cations with fully filled (Lu³⁺) or empty 4f-orbitals (La³⁺, Y³⁺) are not of spectroscopic interest as they do not 74 allow any intra 4f ↔ 4f transitions. However, despite the lack of inherent emission bands, Y³⁺/Lu³⁺/La³⁺ are substantial for 75 various applications due to their capability of host matrix formation²². These ions thus provide a stable and inert surrounding 76 for other activator ions from the RE ion group, such as Nd³⁺ (Nd:YAG lasers) or Ce³⁺ (Ce:YAG/LuAG-based light emitting 77 diodes)^{1,4-7,22}. The comparable ionic radii and electronic structures allow them to form robust crystal lattices that can adopt a 78 wide range of dopant ions to the order of tens of at.%²³. This versatility makes them indispensable in the design of advanced 79 phosphor materials (e.g. LED, solid state lasers), scintillators, and other luminescent materials for lighting, displays, and 80 medical imaging technologies^{1,4-7,22,23}.

82 The primary benefit of optically active rare-earth ions with partially occupied 4f electron orbitals is their spectroscopic 83 stability within the host matrix regardless of whether the matrix consists of the above-described crystalline materials with or 84 without the Y, Lu, La content, amorphous materials or special optical glasses. Emission bands from RE³⁺ ions in the host 85 material closely match their intrinsic energies^{2,4,12}, displaying narrow spectral lines and high cross sections across a broad 86 wavelength range, from UV to MIR. In contrast, transition metals exhibit smaller cross-sections and broader spectral lines due 87 to the significant influence of the host matrix on their 3d shells². This difference occurs because the 4f shells of lanthanides are 88 partially shielded by their outer electron shells (5s and 5p) as is visible in Table 1. This leads to a very weak interaction between 89 these optical active electrons and the host matrix/surrounding ligand field. Perturbation of the local surrounding environment 90 then affects the free RE³⁺ ion Hamiltonian (H_F) and leads to the creation of Stark levels. The Hamiltonian of free RE³⁺ ion can 91 be expressed using Eq.1 as

$$H_F = H_0 + H_C + H_{SO}, \quad (1)$$

92 where the first term, H_0 , represents the nucleus-electron interaction and the kinetic energies of all the electrons, the second 93 term is the coulombic repulsion between electrons, H_C , and the last term describes the spin-orbit interaction, H_{SO} , and thus 94 coupling between the spin angular momentum and the orbital angular momentum. Previously mentioned interaction with the 95 surrounding crystal/ligand field could then be expressed by adding another term representing the perturbation Hamiltonian, 96 V_{LF} , and form the perturbed free ion Hamiltonian for an ion in the host matrix as follows $H = H_F + V_{LF}$. For a more detailed 97 description, please follow Refs.^{2,12,14,15}.

Table 1. Charge configuration of RE³⁺ ions, atomic number (Z), ionic and covalent radii (taken from Ref.²⁴), number of electrons in 4f orbital (n_e), total spin (S) and orbital (L) angular momentum, total angular momentum (J) and derived ^{2S+1}L_J ground spectroscopic term.

Z	Element	Symbol	ER ³⁺ config.	Ionic radius (Å)	Covalent radius (Å)	n_e	S	L	J	Ground term
58	Cerium	Ce	[Kr]4f ¹ 5s ² 5p ⁶	1.02	1.65	1	0.5	3	2.5	² F _{5/2}
59	Praseodymium	Pr	[Kr]4f ² 5s ² 5p ⁶	1.00	1.65	2	1	5	4	³ H ₄
60	Neodymium	Nd	[Kr]4f ³ 5s ² 5p ⁶	0.99	1.64	3	1.5	6	4.5	⁴ I _{9/2}
61	Promethium	Pm	[Kr]4f ⁴ 5s ² 5p ⁶	0.98	1.63	4	2	6	4	⁵ I ₄
62	Samarium	Sm	[Kr]4f ⁵ 5s ² 5p ⁶	0.97	1.62	5	2.5	5	2.5	⁶ H _{5/2}
63	Europium	Eu	[Kr]4f ⁶ 5s ² 5p ⁶	0.97	1.85	6	3	3	0	⁷ F ₀
64	Gadolinium	Gd	[Kr]4f ⁷ 5s ² 5p ⁶	0.97	1.61	7	3.5	0	3.5	⁸ S _{7/2}
65	Terbium	Tb	[Kr]4f ⁸ 5s ² 5p ⁶	1.00	1.59	8	3	3	6	⁷ F ₆
66	Dysprosium	Dy	[Kr]4f ⁹ 5s ² 5p ⁶	0.99	1.59	9	2.5	5	7.5	⁶ H _{15/2}
67	Holmium	Ho	[Kr]4f ¹⁰ 5s ² 5p ⁶	0.97	1.58	10	2	6	8	⁵ I ₈
68	Erbium	Er	[Kr]4f ¹¹ 5s ² 5p ⁶	0.96	1.57	11	1.5	5	7.5	⁴ I _{15/2}
69	Thulium	Tm	[Kr]4f ¹² 5s ² 5p ⁶	0.95	1.56	12	1	5	6	³ H ₆
70	Ytterbium	Yb	[Kr]4f ¹³ 5s ² 5p ⁶	0.94	1.74	13	0.5	3	3.5	² F _{7/2}

98 The electrostatic interaction among electrons then results in the splitting of energy levels by approximately 10⁴ cm⁻¹, 99 leading to the formation of new ^{2S+1}L energy levels separated by the same order of magnitude. Further splitting of these 100 energy levels to new ^{2S+1}L_J levels occurs when spin-orbit coupling is considered. The influence of ligand field perturbations

101 subsequently generates Stark levels, a process referred to as Stark splitting which divides each J level into $2J+1$ new Stark levels
 102 with energy separation of $\approx 10^2 \text{ cm}^{-1}$. Used spectroscopic symbols describe the total spin angular momentum $S = \sum s_i$ and
 103 total orbital angular momentum $L = \sum l_i$ of electron spins s_i and orbital angular momenta l_i for a given electron configuration of
 104 RE^{3+} ion. The term symbol $^{2S+1}L_J$ of the ground state of a multi-electron atom can be found according to three (1)–(3) Hund's
 105 rules, where the lowest energy term is that which (1) has the greatest spin multiplicity and (2) the largest value of the total
 106 orbital angular momentum (at the maximum multiplicity). Spin-orbit coupling then split ^{2S+1}L terms into levels according to the
 107 (3) subshell occupancy. If the subshell is less than half full, the lowest energy belongs to the level with the lowest total angular
 108 momentum value, $J = |L - S|$, and on the opposite, if the subshell is exactly or more than half full, the lowest energy belongs to
 109 the level with the highest total angular momentum value, $J = |L + S|$. This can be demonstrated on the example of Er^{3+} cation
 110 with electron charge configuration of $[\text{Xe}]4f^{11}$ with eleven electrons in $4f$ orbital, where only three are unpaired. By employing
 111 the first and second Hund's rule, the total multiplicity is equal to $S = 1.5$ and the largest total orbital angular momentum is
 112 equal to $L = 6$. Using the standard notation, the letter symbol of total orbital angular momentum $L = S, P, D, F, G, H, I$ corresponds
 113 to $L = 0, 1, 2, 3, 4, 5$ and 6 . According to the third rule, the subshell is more than half full and thus the total angular momentum
 114 value is $J = L + S = 6 + 1.5 = 15/2$. Described procedure thus results in the construction of $^{2S+1}L_J$ ground term for erbium
 115 $3+$ ion as $^4I_{15/2}$. Similar information for other RE ions is listed in Table. 1. Extended energy diagram derived from optical
 116 experiments by Dieke et al.²⁵ is presented in Fig. 2 for the subset of $^{2S+1}L_J$ multiplets and energies up to $\approx 5 \text{ eV}$ ($\approx 40\,000$
 117 cm^{-1} or $\approx 250 \text{ nm}$). Presented energy levels are placed across the wavelength range covered by commonly used spectroscopic
 118 techniques and thus covers only a low-energetic part of the energy level diagram (see Fig. 2) for the complete set of $^{2S+1}L_J$
 119 multiplets for each RE^{3+} ion, which was later completed using the theoretical calculations by Peijzel et al.²⁶

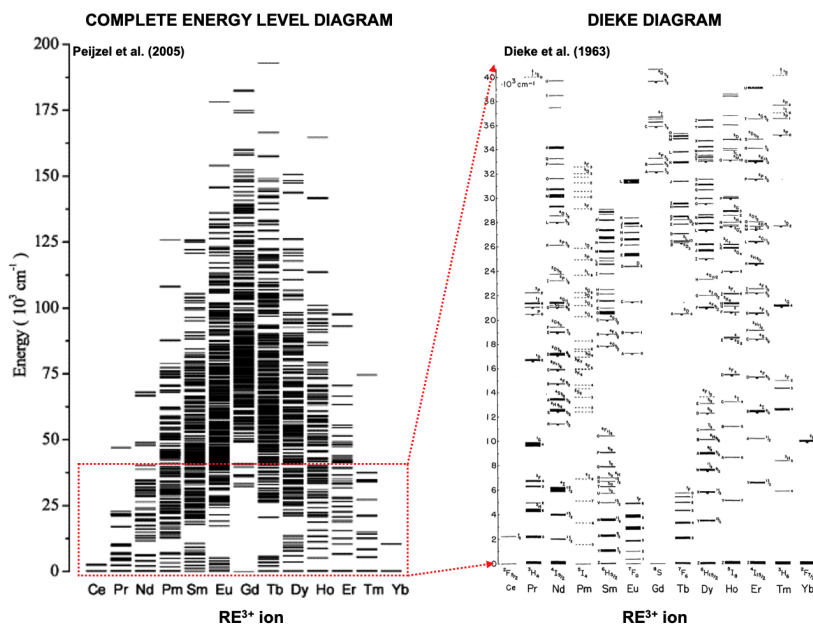


Figure 2. Energy level diagram of RE^{3+} ions for the calculated complete set of $^{2S+1}L_J$ multiplets²⁶ (left) and the classical experimentally determined "Dieke"²⁵ diagram for energies up to $40\,000 \text{ cm}^{-1}$ (right).

120 Judd-Ofelt theory

121 JO theory was introduced independently to each other by Brian R. Judd¹⁴ and George S. Ofelt¹⁵ in 1962 based on the previous
 122 work of J.H. Van Vleck about spectroscopic properties of rare-earth ions in solids²⁷. Sharp spectroscopic lines of RE^{3+} ion
 123 implicated the intra- $4f$ electronic transitions that occur between the levels inside the $4f$ electronic shell. This is, however,
 124 forbidden by the Laporte selection rule which says that states with even parity can be connected by electric dipole transitions
 125 only with states of odd parity and the same in vice versa. Among the other proposed but incorrect explanations based on (1)
 126 $4f$ to $5d$ transitions or (2) magnetic dipole or electric quadrupole radiation, Van Vleck²⁷ and Broer²⁸ presented a reasonable
 127 solution based on the distortion of the electronic motion by surrounding crystal/ligand field in the material. Presented distortions
 128 then bypass the Laporte selection rule and allow the electric dipole radiation even for intra- $4f$ electronic transitions. However,
 129 to disturb the wavefunctions and negate the Laporte rule, the external field must also be noncentrosymmetric. From this point,

130 about a quarter of a decade later and with further advances in algebra, computing, and increased applications of lasers, JO^{14,15}
 131 theory was presented and described the induced electric dipole transitions of RE³⁺ ions in host materials.

132 JO theory then provides a theoretical expression for the calculation of electric-dipole-induced (ED) oscillator strengths, f_{ED}^{abs}
 133 (Eq. 2), as the ratio between absorbed (emitted) and emitted (absorbed) intensity of electromagnetic radiation for harmonically
 134 oscillating electron and expresses the probability of individual $J \leftrightarrow J'$ transition as follows,

$$f_{ED}^{abs}(J \rightarrow J') = \frac{8\pi^2 m_e c}{3h\bar{\lambda}(2J+1)} n \left(\frac{n^2+2}{3n} \right)^2 \sum_{i=2,4,6} \Omega_i |\langle (S,L)J | U^i | J'(S',L') \rangle|^2, \quad (2)$$

$$f_{MD}^{abs}(J \rightarrow J') = \frac{h}{6m_e c \bar{\lambda}} \frac{n}{(2J+1)} |\langle (S,L)J | L + gS | J'(S',L') \rangle|^2, \quad (3)$$

135 where J and J' are the quantum numbers of the initial ground state and excited state, respectively, n is the refractive index, h
 136 is the Planck's constant, m_e is electron mass, c is the speed of light in vacuum, $\bar{\lambda}$ is the mean wavelength of corresponding $J \rightarrow J'$
 137 transition and Ω_i are the JO parameters for $i = 2, 4, 6$. The terms in brackets are the squared reduced matrix elements, which
 138 are almost independent on the host matrix. Note, that the summation over i is also known as manifold linestrength which will
 139 be introduced later in this section. Compared to the ED-induced absorption, the magnetic-dipole (MD) transitions are usually
 140 orders of magnitude smaller. However, some MD transitions can make a significant contribution to the total oscillator strength,
 141 f_{total}^{abs} . The MD-induced oscillator strength, f_{MD}^{abs} , for $J \rightarrow J'$ is then expressed via Eq.3 and unlikely ED-induced transitions
 142 does not contain any intensity scaling parameter^{12,29}. The reduced matrix element for each transition in Eq. 3 is calculated
 143 using procedure described in Refs.^{2,12,30} and are nonzero only if $S = S'$ and $L = L'$ while $J = J', J = J' + 1$, and $J = J' - 1$. On
 144 the example of Er-doped materials, only the fundamental absorption ${}^4I_{15/2} \rightarrow {}^4I_{13/2}$ (≈ 1550 nm) contributes significantly. As a
 145 result, the magnetic-dipole contribution can account for up to one-third of the total oscillator strength³¹. The total theoretical
 146 oscillator strength for transitions which contains both ED and MD is thus given as $f_{total}^{abs}(J \rightarrow J') = f_{ED}^{abs}(J \rightarrow J') + f_{MD}^{abs}(J \rightarrow J')$.
 147 Interaction between the surrounding host matrix and RE³⁺ ions are then expressed by the set of three JO phenomenological
 148 parameters, which can be obtained by equating the expressions for the experimental (f_{exp}) and theoretical (f_{total}^{abs}) oscillator
 149 strengths using the least-squares method, including both ED+MD or only ED contribution. The experimental oscillator strengths
 150 can be calculated from optical absorption spectra using the Eq.4,

$$f_{exp}(J \rightarrow J') = \frac{2m_e c}{\alpha_f h \bar{\lambda}^2 N} \int \alpha(\lambda) d\lambda, \quad (4)$$

151 where α_f is fine structure constant, N is rare-earth ion concentration and $\alpha(\lambda)$ is wavelength-dependent absorption
 152 coefficient. Optical absorption can be also expressed using the absorption cross section, σ_{abs} , defined as $\sigma_{abs} = \alpha(\lambda)/N$.

153 Using knowledge of the JO parameters, several important spectroscopic quantities can be calculated for a specific material
 154 system, such as the transition probabilities, $A(J', J)$, radiative lifetimes, τ^{JO_r} , or the luminescence branching ratios, $\beta(J', J)$.
 155 The transition probabilities for each transition are calculated from Eq. 5:

$$A(J' \rightarrow J) = \frac{64\pi^4 e^2}{3h\lambda_B^3(2J'+1)} (\chi_{ED} S_{ED} + \chi_{MD} S_{MD}), \quad (5)$$

156 where J' is the total angular momentum of the upper excited state, λ_B is the transition wavelength (also called Barycenter),
 157 S_{ED} and S_{MD} are electric and magnetic dipole line strengths and χ_{ED} and χ_{MD} are the local field corrections of the electric
 158 dipole (Eq.6) and the local field correction of the magnetic dipole (Eq.7).

$$\chi_{ED} = n \left(\frac{n^2+2}{3} \right)^2, \quad (6)$$

$$\chi_{MD} = n^3, \quad (7)$$

159 The electric dipole linestrength is then easily calculated from each excited state manifold to lower lying manifold using the
 160 JO parameters and matrix elements by Eq. 8:

$$S_{ED} = \sum_{i=2,4,6} \Omega_i |\langle (S,L)J | U^i | J'(S',L') \rangle|^2, \quad (8)$$

where e is unit charge of electron. The magnetic dipole line strengths are given by Eq. 9:

$$S_{\text{MD}} = \left(\frac{h}{4\pi m_e c} \right)^2 |\langle (S, L)J | \hat{L} + g\hat{S} | J'(S', L') \rangle|^2, \quad (9)$$

where g is the electron g -factor ($g \approx 2.002$) and the terms in brackets are reduced matrix elements of the $|L + gS|$ operator. The radiative lifetimes of each level, $\tau_{\text{r}}^{\text{JO}}$, are then calculated from the transition probabilities using Eq.10. The luminescence branching ratio, $\beta(J', J)$ is given by Eq.11 and represents the distribution of the emission transitions in the emission spectra. Combining the theoretical JO lifetime and branching ratio with the experimentally measured lifetime, τ_{r} , for a designated transition results in Eq.12, which defines the radiative quantum yield, η , of the corresponding $J' \rightarrow J$ electronic transition.

$$\tau_{\text{r}}^{\text{JO}} = \frac{1}{\sum_{J'} A(J', J)}, \quad (10)$$

$$\beta(J', J) = \frac{A(J', J)}{\sum_{J'} A(J', J)}, \quad (11)$$

$$\eta(J', J) = \frac{\tau_{\text{r}}}{\tau_{\text{r}}^{\text{JO}}} \beta(J', J), \quad (12)$$

The quality of the least-squares fit can be quantified by the RMS parameter, expressed by Eq. 13 or Eq. 14, respectively:

$$RMS_f = \sqrt{\frac{\sum (f_{\text{exp}} - f_{\text{total}}^{\text{abs}})^2}{T - 3}}, \quad (13)$$

$$RMS_S = \sqrt{\frac{\sum (S_{\text{exp}} - S_{\text{total}})^2}{T - 3}}, \quad (14)$$

where T is the number of transitions used for the calculation.

Judd-Ofelt theory: Experimental practice

From the experimental perspective, accurate spectroscopic characterization of the prepared materials is essential for the proper application of the JO theory and estimation of JO parameters, transition probabilities and derived values of branching ratios and theoretical luminescence lifetimes.

The first step of the JO analysis requires the measurement of the transmission spectrum, $T(\lambda)$, to determine the wavelength-dependent values of the absorption coefficient, $\alpha(\lambda)$, and then the values of the absorption cross-section, $\sigma_{\text{abs}}(\lambda)$. Although the calculation of the $\sigma_{\text{abs}}(\lambda)$ value from the absorption coefficient using the known RE^{3+} ion concentration (N) is relatively simple, where $\sigma_{\text{abs}}(\lambda) = \alpha_{\text{k}}(\lambda)/N$, the calculation of the absorption coefficient may vary across the literature depending on whether scattering losses are not included (15), included (16) and if taking into account multiple reflections in plane parallel geometry of the sample (17) (in the case of solids). As is visible from Fig.3 in the example of Er^{3+} -doped glass, the spectral shape of corresponding transitions in the transparent region is practically identical with significant offset caused by the not included/included reflectivity (R). In cases where the absorption band is offset from the zero $\sigma_{\text{abs}}(\lambda)$ value or overlaps with the absorption edge, it is therefore necessary to subtract the background to obtain the most possible accurate value. If the number of observed manifolds is sufficient, it is recommended to exclude the transitions within the absorption edge from the calculation of the JO parameters to increase fit accuracy.

$$\alpha_1 = \frac{-1}{l} \ln(T) = \frac{-2.303 \log_{10}(T)}{l} \quad (15)$$

$$\alpha_2 = \frac{-1}{l} \ln\left(\frac{T}{(1-R)^2}\right) = \frac{2.303 [-\log_{10}(T) + \log_{10}(1-R)^2]}{l} \quad (16)$$

$$\alpha_3 = \frac{1}{l} \ln \left[\frac{(1-R)^2 + \sqrt{(1-R)^4 + 4R^2 T^2}}{2T} \right] \quad (17)$$

184 Derived spectral dependence of the $\sigma_{\text{abs}}(\lambda)$ is used for estimation of the integrated absorption cross section, $\int_{J \rightarrow J'} \sigma_{\text{abs}}(\lambda) d\lambda$
 185 (in $\text{cm}^2 \text{ nm}$), for each manifold (Fig.3b) which is then used for calculation of the experimental oscillator strength (Eq.4) or
 186 experimental linestrength (Eq.18) according to

$$S_{\text{exp}}(J \rightarrow J') = \frac{3ch(2J+1)}{8\pi^3 e^2 \bar{\lambda}} n \left(\frac{3}{n^2 + 2} \right)^2 \int_{J \rightarrow J'} \sigma(\lambda) d\lambda, \quad (18)$$

187 where J is the quantum number representing the total angular momentum of the original ground state, found from the $^{2S+1}L_J$
 188 term constructed by using the three Hund's rules (see previous section for detailed description). As the linestrength is typically
 189 referred in cm^2 , the units and input values for other quantities and constants in presented calculations are used as follows: speed
 190 of light, $c = 3 \times 10^{10} \text{ cm s}^{-1}$, Planck constant, $h = 6.626 \times 10^{-30} \text{ cm}^2 \text{ kg s}^{-1}$, unit charge of electron, $e = 1.5189 \times 10^{-11} \text{ cm}^{3/2}$
 191 $\text{kg}^{1/2} \text{ s}^{-1}$, fine structure constant, $\alpha = 7.297 \times 10^{-3} \approx 1/137$, and electron mass, $m_e = 9.11 \times 10^{-11} \text{ kg}$. The last presented
 192 parameter, mean wavelength ($\bar{\lambda}$), can be found as well from the absorption cross section data using the harmonic, $\bar{\lambda}_H$ (Eq.19a),
 193 or weighted mean value, $\bar{\lambda}_W$ (Eq.19b), for each transition as is illustrated in Fig.3b. Both derived mean values lead to almost
 194 similar results, which, however, may differ from the value of simply subtracting absorption band maximum, λ_{max} . Note, that for
 195 the proper calculation of experimental oscillator strength or experimental linestrength, the values of experimentally determined
 196 integrated cross section and mean wavelength must be recalculated after subtraction from the graph and used in ($\text{cm}^2 \text{ cm}$) and
 197 (cm), respectively.

$$(a) \bar{\lambda}_H = \frac{1}{\frac{\sum \lambda \sigma_{\text{abs}}(\lambda)}{\sum \sigma_{\text{abs}}(\lambda)}} = \frac{\sum \sigma_{\text{abs}}(\lambda)}{\sum \lambda \sigma_{\text{abs}}(\lambda)} \text{ or } (b) \bar{\lambda}_W = \frac{\sum \sigma_{\text{abs}}(\lambda) \lambda}{\sum \sigma_{\text{abs}}(\lambda)} \quad (19)$$

198 By completing all of the above characteristics, the JO phenomenological parameters, $\Omega_i (i = 2, 4, 6)$ are determined by
 199 fitting the experimental absorption represented by experimental oscillator strength (Eq.4) or linestrength (Eq.18) using the
 200 least square method to the theoretical ones considering only the electric-dipole contribution ($f_{\text{total}}^{\text{abs}} = f_{ED}^{\text{abs}}$ or $S_{\text{total}} = S_{ED}^{\text{abs}}$) or
 201 both electric/magnetic-dipole contributions ($f_{\text{total}}^{\text{abs}} = f_{ED}^{\text{abs}} + f_{MD}^{\text{abs}}$ or $S_{\text{total}} = S_{ED} + S_{MD}$). On the example of the second case,
 202 experimental and theoretical linestrengths are written in their respective matrix forms similarly as described in Ref.² and the
 203 sum of the square difference is minimized. Since the JO theory includes only three parameters, more than three absorption
 204 manifolds have to be provided for calculation, and thus JO theory cannot be applied to single Yb^{3+} -doped materials. After
 205 fitting procedure, materials characteristics, such as $A(J', J)$, $\beta(J', J)$ and τ^{JO} , are calculated using the known JO parameters
 206 from Eq.5, Eq.10 and Eq.11. Nevertheless, for proper calculation of transition probabilities (Eq.5), it is also necessary to
 207 know the value of corresponding transition ($J' \rightarrow J$) wavelength from an excited state to the ground/lower-energy state, λ_B ,
 208 also commonly referred as Barycenter. This value should be in principle different from the mean wavelength $\bar{\lambda}$ or absorption
 209 band maximum (λ_{max}). However, the assignment of the barycenter varies considerably within the literature (or is not clearly
 210 explained) and can be divided into three main approaches, using the (1) similar value of mean wavelength $\bar{\lambda}$ derived from the
 211 optical absorption measurements as Barycenter or (2) tabulated values assigned with U^2, U^4, U^6 elements regardless of the host
 212 material or (3) the peak/mean wavelength derived from emission spectra at room temperature. Using the last approach, it is
 213 possible to estimate the spectral shift between mean absorption and emission wavelength for one transition and then apply this
 214 difference to all other transitions. Given the extensive nature of the topic, it is up to the author which approach is chosen and
 215 which would best fit the experimental results.

216 Combinatorial Judd-Ofelt theory

217 Following the previous section, it is clear that the selection of the appropriate transition bands, their experimental description
 218 or the decision whether to take into account the magnetic-dipole correction are crucial for accurate calculation of the JO
 219 parameters^{2, 12, 31}. Judd-Ofelt analysis then minimizes the square of the difference between theoretical ($f_{\text{total}}^{\text{abs}}$ or S_{total}) and
 220 experimentally obtained (f_{exp} or S_{exp}) oscillator strengths/linestrengths in the form described above and using the corresponding
 221 $\Omega_i (i = 2, 4, 6)$ as an adjustable parameters. To compute the JO parameters, at least four experimentally measured absorption
 222 manifolds must be used. When a larger set of measured absorption bands is available, it becomes possible to exclude certain
 223 transitions (e.g., those exhibiting hypersensitivity) or to limit the JO analysis to transitions within a specific spectral region, for

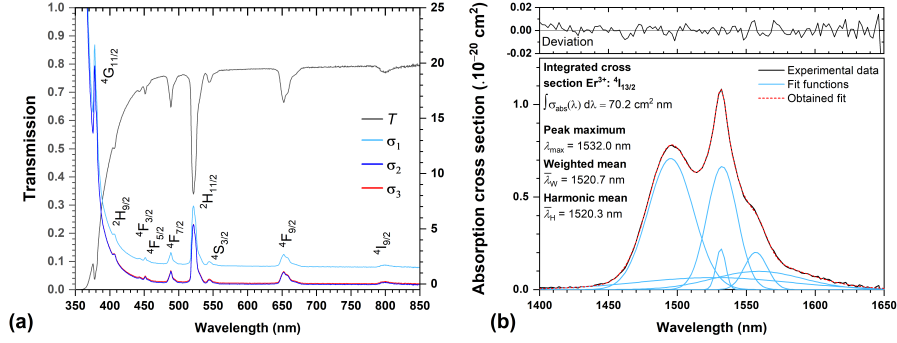


Figure 3. a) Transmission spectrum and corresponding absorption cross sections, employing various corrections on scattering losses or plane parallel geometry of the sample; b) example of integrated area calculation of a selected band.

224 example, due to experimental limitations or the presence of fundamental absorption of the host matrix. However, for accurate
 225 determination of the complete set of all three JO parameters, the following criteria must be met: (1) the involved transitions
 226 must have non-zero values of the corresponding reduced squared matrix elements U^i ($i = 2, 4, 6$), (2) these values should be of
 227 the same order of magnitude, and (3) at least three transitions that satisfy the previous two conditions must be used.

228 As a result, various studies exclude hypersensitive transitions, such as the ${}^2H_{11/2}$ transition for Er^{3+} ions with a high
 229 U^2 value, do not cover the full spectral range due to the lack of experimental capability to measure absorption bands in the
 230 NIR/MIR regions (Nd^{3+} (${}^4I_{11/2}$), Dy^{3+} (${}^6H_{13/2}$), Sm^{3+} (${}^6H_{7/2}$ and ${}^6H_{9/2}$), etc), include/exclude the transitions with magnetic-
 231 dipole contribution or selectively include/exclude transitions affected by the absorption edge. This last scenario can be
 232 particularly limiting for materials with low optical transmission in the visible spectral region, such as chalcogenide glasses,
 233 since this region typically contains the majority of experimentally observable absorption bands associated with rare-earth ions.
 234 For some materials, it is therefore in principle necessary to include the transitions affected by the absorption edge, otherwise
 235 they would not meet the condition for the minimum number of used manifolds. Using Combinatorial Judd-Ofelt analysis
 236 (C-JO)³¹ and a higher than minimum number of transitions, it is thus possible to identify those manifold combinations that
 237 enable accurate JO analysis ensuring consistent and reliable results. Moreover, by employing various types of host materials
 238 and broad-spectrum analysis for each rare-earth ion it will be possible to identify such critical combinations, which are essential
 239 for the calculation of JO parameters and thus should not be omitted. The total value of all possible combinations then depends
 240 on the number of input absorption bands (N_B) according to Eq.20

$$\text{Total combinations} = \sum_{r=k}^{N_B} \binom{N_B}{r} \quad (20)$$

241 where k is the minimum number of elements in each combination (from 4 to N_B) and $\binom{N_B}{r}$ is the binomial coefficient
 242 calculated as $\binom{N_B}{r} = \frac{N_B!}{r!(N_B-r)!}$. It is then possible to obtain 5, 22, 64, 163, 382 and 848 possible combinations for original sets
 243 composed of 5, 6, 7, 8, 9 and 10 experimentally obtained absorption bands. The obtained set of all possible combinations
 244 can be subsequently reduced by inappropriate combinations using different empirical approaches (e.g. due to unphysicality
 245 of partial solutions or non-converging results when calculating JO parameters) or using the analysis of statistical distribution
 246 of the resulting JO parameter values depending on the absorption bands used³¹. In order to eliminate the empirical selection
 247 approach, the box/whisker plot statistical method may be applied to the original set of all possible combinations reduced by the
 248 non-physical cases (negative values of JO parameters)³¹. According to the used statistical model, data points (combinations)
 249 outside the whisker boundaries are identified as outliers and thus may be excluded from the dataset as was shown in Ref.³¹ on
 250 the example of Er^{3+} -doped materials. Several other examples of presented C-JO analysis are given in the following section
 251 *Computational Validation: Judd-ofelt analysis and Combinatorial Judd-Ofelt analysis.*

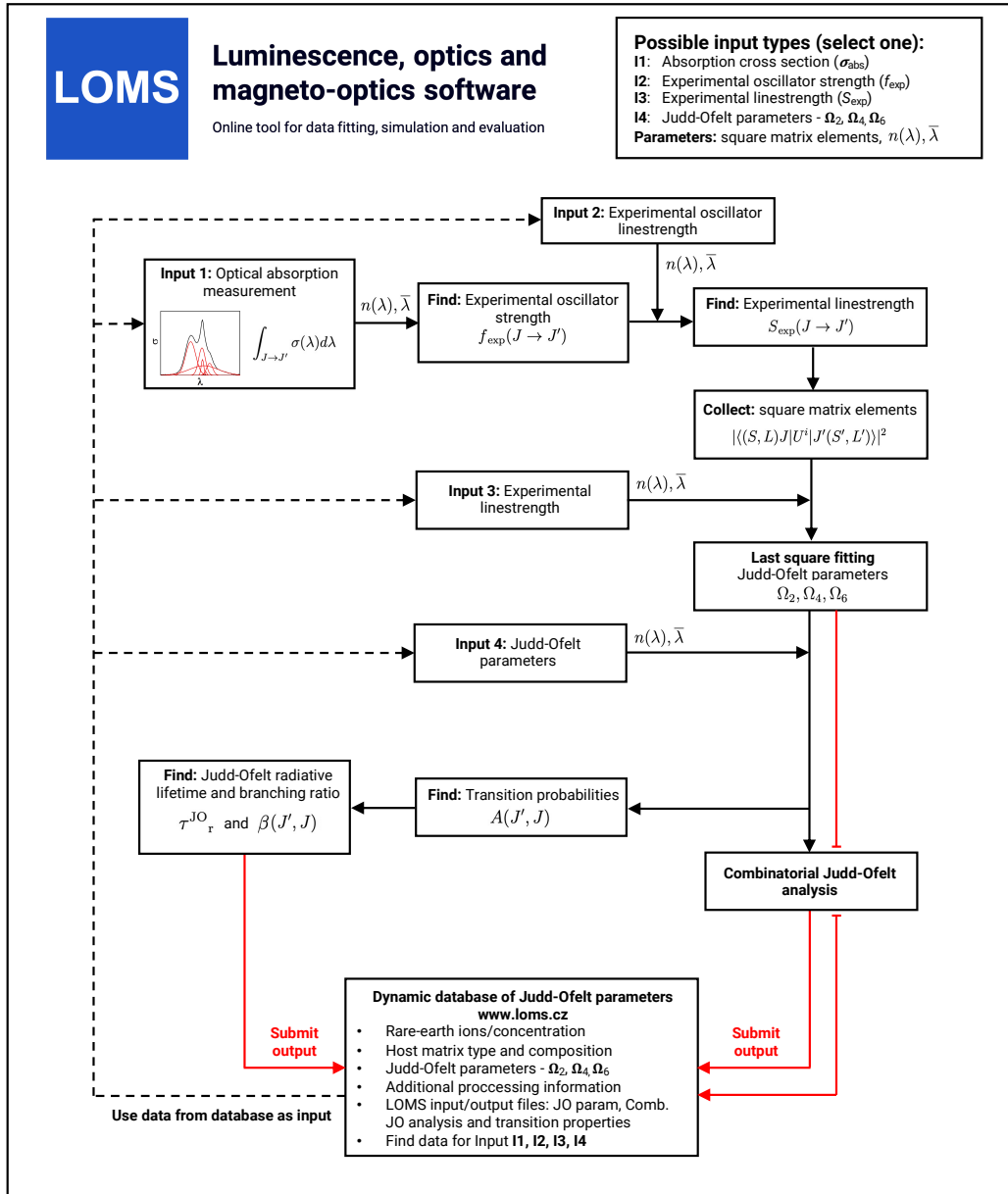


Figure 4. Software procedure of Judd-Ofelt analysis and implementation of Judd-Ofelt parameters database.

252 Evaluation protocol and graphical software interface

253 The process of JO and Combinatorial JO analysis using the Luminescence, optics and magneto-optics software (LOMS)
 254 (www.LOMS.cz or www.LOMS.cz/jo) is outlined in the attached flowchart (Fig.4), while the graphical user interface of LOMS
 255 computational tool is shown in Fig.5. To enhance versatility, users can choose from four recommended input options, depending
 256 on the desired level of data processing and verification (Fig.5, Radio button: *Input values*). The software supports direct
 257 processing of experimental oscillator strength/linestrength input data, enabling straightforward comparison with experimental
 258 results from the literature. Additionally, a magnetic-dipole correction feature is available for input data in the form of absorption
 259 cross sections, which can be applied by selecting Radio button: *Use magnetic dipole correction*. Furthermore, the software
 260 allows for direct input of JO parameters, followed by the calculation of material radiative characteristics. The list of possible
 261 input files is as follows:

- 262 1. Integrated absorption cross section $\int \sigma_{\text{abs}} d\lambda$ (in $\text{cm}^2 \text{ nm}$) or
- 263 2. Experimental oscillator strength, f_{exp} , taken from an external source or calculated using Eq.4 or
- 264 3. Experimental linestrength, S_{exp} (in cm^2), taken from an external source or calculated using Eq.18 or
- 265 4. Judd-Ofelt parameters, $\Omega_2, \Omega_4, \Omega_6$, (in cm^2), taken from an external source or calculated using aforementioned procedure.

266 Furthermore, to successfully calculate JO parameters and radiation material characteristics (transition probabilities, radiative
 267 lifetimes and branching ratios), the input file must be supplemented with the following data sets for each experimentally derived
 268 manifold:

- 269 1. Refractive index (Fig.5, Radio button: *Refractive index values*) and
- 270 2. Mean peak wavelength (in nm) derived using Eq.19 for each placed transition (Fig.5, Text field: *Mean peak wavelength*)
- 271 3. Square matrix elements U^2, U^4, U^6 for each placed transition (Fig.5, Text fields: U_2, U_4, U_6)
- 272 4. Barycenter: (in cm^{-1}) for each transition. If they are not experimentally detectable, it is necessary to use their tabulated
 273 values or choose one of the approaches discussed further in this section (Fig.5, Text fields: *Barycenter*).

The screenshot shows the LOMS online tool interface. At the top, there is a navigation bar with the LOMS logo and links for 'Judd-Ofelt analysis v1.0', 'JO parameter database', 'User guide', 'About LOMS', and 'info@loms.cz'. Below this is a sample name field containing 'reference_er_sigma_Hrabovsky2024'. There are radio buttons for 'Use magnetic dipole correction' (with sub-options FED and FED+MD) and 'Input values' (with sub-options Integrated cross section, JO parameters, Refractive index values, and Direct + Sellmeier). A table for inputting transition data is visible, with columns for 'Excited state', 'U2', 'U4', 'U6', 'Integrated cross section (cm²·nm)', 'Mean peak wavelength (nm)', 'Refractive index', 'F_{exp}', 'S_{exp} (cm²)', 'S_{code} (cm²)', and 'Barycenter (cm⁻¹)'. Below the table is a 'Data import' section with a 'Choose File' button, an 'Import file' button, and links for 'Example data' and 'Data template'. At the bottom, there are buttons for 'Calculate JO parameters', 'Combinatorial JO analysis', and 'Transition analysis'. A footer contains a Creative Commons license notice and a help icon.

274 **Figure 5.** The graphical user interface of LOMS online tool, which is available at <https://www.LOMS.cz/>.

275 The refractive index can be added directly as defined values for each transition in the same row (Fig.5, Text field: *Refractive index*) or expressed using a standard two-term Sellmeier model (Eq.21)

$$n^2 = A + \frac{B_1 \lambda^2}{\lambda^2 - C_1} + \frac{B_2 \lambda^2}{\lambda^2 - C_2}, \quad (21)$$

276 where the A , B_1 , C_1 , B_2 and C_2 are the Sellmeier coefficients. Note, that while refractive index values can be entered directly -
 277 sufficient for calculation of JO parameters - determining the radiative characteristics, such as $A(J', J)$, $\beta(J', J)$ and τ^{JO}_r , requires
 278 specifying its spectral dependence via the appropriate Sellmeier coefficients. If the refractive index of the material is not readily
 279 available, it can be sourced from publicly accessible databases, such as *refractiveindex.info*³². A consistent set of tabulated
 280 matrix elements for all RE elements listed in Table 1 and default values of barycenters and mean peak wavelengths are provided
 281 (see Figshare repository³³ or www.LOMS.cz) with the possibility of their interactive editing in the software GUI if necessary. A
 282 key feature of the software is the ability to dynamically select the number of included transitions — via a column of checkboxes
 283 on the left side in Fig.5) - without requiring modifications to the input data structure. Once all the above requirements have
 284 been met, the classical JO analysis can be performed via pressing button *Calculate JO parameters*, while a Combinatorial JO
 285 analysis - evaluating all possible combinations of inserted absorption bands - can be executed using the *Combinatorial JO*
 286 *analysis* button. The GUI structure displaying the results is shown in Fig.6. Displayed results of C-JO analysis further contain
 287 information regarding the median of JO parameters and min/max values of radiative lifetimes from the lowest energy level for
 288 different datasets: (1) Full set: contains all absorption bands, $k = N_B$ in Eq.20, (2) All combinations: $k \in \langle 4, N_B \rangle$, (3) Reduced
 289 (only positive): set of data without discarded combinations, where at least one JO value is negative and (4) Reduced (Box plot):
 290 reduced set of all combinations using the Box plot method similarly as in Ref³¹. Radiative lifetimes are also included for each
 291 used combination of absorption bands in data export file together with values of RMS_f and RMS_S .

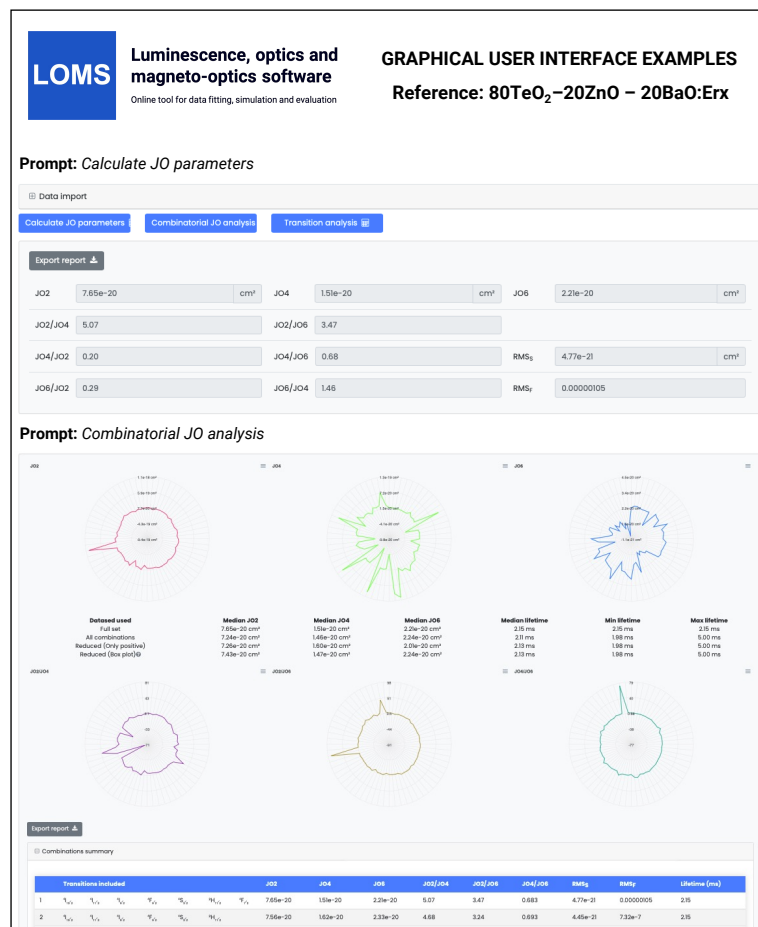


Figure 6. The graphical user interface of LOMS online tool (<https://www.LOMS.cz>): Illustrative example of results structure for classical and combinatorial Judd-Ofelt analysis.

Note, that in many cases, two or more closely located transitions may overlap with each other and therefore it is not possible to easily distinguish their independent contribution. This can be the example of two absorption bands ${}^2\text{H}_{11/2}$ (≈ 530 nm) and ${}^4\text{S}_{3/2}$ (≈ 550 nm) in Er^{3+} -doped materials. In such cases, it is therefore necessary to apply a modified procedure for the calculation of JO parameters as follows: (1) estimate the combined integrated absorption cross section which involves both absorption bands, (2) estimate the mean peak wavelength in the same way as if it was a single absorption band, (3) sum the respective matrix elements of all the participating transitions into one and (4) write them to the LOMS.cz online GUI in one line - choose the line of one of the involved transitions (or similarly in input .csv file). This modified procedure then affects the U2, U4, U6, integrated cross section and mean wavelength cells. For better clarity, the difference is visible in Fig.(7) and the data repository³³ also contains .xls reference file with shown calculation process. It is also important to note, that it is necessary to uncheck the remaining transitions so that only the one combined transition/row participates in the calculation. This then acts as the combined level of ${}^2\text{H}_{11/2} + {}^4\text{S}_{3/2}$. It is then necessary to remember that in the output file of the JO analysis and the combinatorial JO analysis, this transition no longer represents only one level, but a combination of all involved manifolds. However, this no longer applies to the calculation of radiative transitions properties (A , β , τ), which is done separately and independently of whether the combined or single bands were used for the calculation of JO parameters or not. This is of course due to the fact that radiative properties are calculated directly from the JO parameters, i.e. energy level assignment in *Transition analysis* section is independent of the structure of the data input.

No overlaps										
Excited state	U2	U4	U6	Integrated cross section (cm ² /nm)	Mean peak wavelength (nm)	Refractive index	F _{exp}	S _{exp} (cm ²)	S _{calc} (cm ²)	Barycenter (cm ⁻¹)
${}^4\text{S}_{3/2}$										109
${}^2\text{H}_{11/2}$	0.0194984	0.1173353	1.4316383	7e-19	1520	1.9986	0.000003429	3.846e-20	3.491e-20	6570
${}^4\text{S}_{3/2}$	0.0281916	0.0003049	0.3952644	9.41e-20	974	2.0099	0.000001223	7.993e-21	1.090e-20	10202
${}^2\text{H}_{11/2}$	0.188329	0	0.0099097	3.41e-20	801	2.0184	6.015e-7	3.494e-21	9.289e-21	1242
${}^4\text{S}_{3/2}$	0	0.5353863	0.4817945	1.48e-19	655	2.0349	0.000003904	1.831e-20	1.829e-20	15227
${}^2\text{H}_{11/2}$	0	0	0.221383	1.95e-20	544	2.0579	7.458e-7	2.849e-21	4.888e-21	18359
${}^4\text{S}_{3/2}$	0.712554	0.4123647	0.0924666	4.21e-19	521	2.0652	0.00001765	6.384e-20	6.285e-20	1910
${}^2\text{H}_{11/2}$	0	0.1468776	0.6285381	6.53e-20	489	2.0775	0.000003091	1.044e-20	1.607e-20	20448

Theoretical overlaps between ${}^4\text{S}_{3/2}$ and ${}^2\text{H}_{11/2}$										
Excited state	U2	U4	U6	Integrated cross section (cm ² /nm)	Mean peak wavelength (nm)	Refractive index	F _{exp}	S _{exp} (cm ²)	S _{calc} (cm ²)	Barycenter (cm ⁻¹)
${}^4\text{S}_{3/2}$										109
${}^2\text{H}_{11/2}$	0.0194984	0.1173353	1.4316383	7e-19	1520	1.9986	0.000003429	3.846e-20	3.533e-20	6570
${}^4\text{S}_{3/2}$	0.0281916	0.0003049	0.3952644	9.41e-20	974	2.0099	0.000001223	7.993e-21	1.098e-20	10202
${}^2\text{H}_{11/2}$	0.188329	0	0.0099097	3.41e-20	801	2.0184	6.015e-7	3.494e-21	8.948e-21	1242
${}^4\text{S}_{3/2}$	0	0.5353863	0.4817945	1.48e-19	655	2.0349	0.000003904	1.831e-20	1.813e-20	15227
${}^2\text{H}_{11/2}$	0.712554	0.4123647	0.318029	4.4051e-19	523	2.0645	0.00001823	6.658e-20	6.564e-20	18359
${}^4\text{S}_{3/2}$	0.712554	0.4123647	0.0924666	4.21e-19	521	2.0652	0.00001765	6.384e-20	6.067e-20	1910
${}^2\text{H}_{11/2}$	0	0.1468776	0.6285381	6.53e-20	489	2.0775	0.000003091	1.044e-20	1.621e-20	20448

Figure 7. The graphical user interface of LOMS online tool, with shown comparison between data input structure without and with observed absorption band overlap. See the main text for discussion.

Results of transition analysis, calculation of $A(J', J)$, $\beta(J', J)$, τ^{JO} , A_{ED} , A_{MD} , will be displayed after pressing the *Transition analysis* button (see Fig.5). The results structure for radiative transition analysis in GUI is shown in Fig.8 and the structure of example output file is visible from Table2. Note, that for successful transition analysis, it is also necessary to include the Barycenter values for each transition and not only for those which were inserted. It is because the transition probabilities, $A(J', J)$ (Eq.5), are calculated for each transition ($J' \rightarrow J$) from an excited state to the ground/lower-energy state. As was discussed in the section *Judd-Ofelt theory: Experimental practice*, the barycenter value should be in principle different from the mean wavelength $\bar{\lambda}$ or absorption band maximum (λ_{max}) as the position of photoluminescence emission is usually red-shifted compared to position of optical absorption (this is valid for both peak/mean wavelength values). However, the assignment of the barycenter varies considerably within the literature (or is not clearly explained) and can be divided into three main approaches, using the (1) similar value of mean wavelength $\bar{\lambda}$ derived from the optical absorption measurements as Barycenter or (2) tabulated values assigned with U², U⁴, U⁶ elements regardless of the host material or (3) the peak/mean wavelength derived from emission spectra at room temperature. To avoid limiting of the calculation, the software allows all the above-mentioned options depending on the selected value. The LOMS.cz software then calculates the energy difference between selected energy levels, which will be used for the calculation of transition probabilities (Eq.5). The barycenter values may be then inserted as follows:

- Barycenter value similar to mean wavelength:** (1) leave the first box for the ground state in Barycenter column (Fig.5, Text fields: *Barycenter*) blank or equal to zero, (2) fill the other positions with corresponding recalculated values of mean wavelength in cm^{-1} ($\text{cm}^{-1} = 10^7/\text{nm}$)
- Tabulated values of Barycenter:** fill the corresponding manifold cell for each transition using the tabulated values.

326 3. **Barycenter value with the constant shift:** according to software procedure (JOFwin2011) presented by Walsh², it is
 327 possible to insert the offset position of the ground state which more or less represents the energy spectral shift between
 328 optical absorption and emission band peak/mean maximum. In this case, the value in the first box for the ground state
 329 in Barycenter column contains the value of this energy spectral shift, whereas the other values represents the mean
 330 wavelengths (in cm^{-1}) derived from optical absorption spectra.

331 Using the last approach, it is possible to estimate the spectral shift between mean absorption and emission wavelength for
 332 one transition and then apply this difference to all other transitions. Given the extensive nature of the topic, it is up to the author
 333 which approach is chosen and which would best fit the experimental results.

LOMS Luminescence, optics and magneto-optics software
 Online tool for data fitting, simulation and evaluation

GRAPHICAL USER INTERFACE EXAMPLES
 Reference: 80TeO₂-20ZnO - 20BaO:Er_x

Prompt: Transition analysis

Export report ↓

Transitions summary

Transition	Wavelength (nm)	s(IJ)	s(MJ)	A(IJ)	A(MJ)	Beta	Lifetime (ms)
4i3/2 - 4i5/2	1547.7	3.49e-20	1.62e-42	388	78.3	1.00	2.14
4i1/2 - 4i5/2	990.8	1.09e-20	0.00	550	0.00	0.867	1.58
4i1/2 - 4i3/2	2753.3	2.91e-20	1.79e-42	66.5	17.7	0.133	31.9
4i9/2 - 4i5/2	812.8	2.84e-21	0.00	316	0.00	0.626	1.98
4i9/2 - 4i3/2	1717.7	1.60e-20	0.00	184	0.00	0.384	5.30
4i9/2 - 4i1/2	4524.9	4.05e-21	9.03e-43	2.50	2.42	0.00973	204
4f9/2 - 4i5/2	661.0	1.83e-20	0.00	3.80e+3	0.00	0.895	0.229
4f9/2 - 4i3/2	1153.8	4.67e-21	0.00	177	0.00	0.0407	2.18
4f9/2 - 4i1/2	1886.1	3.39e-20	4.30e-43	249	13.7	0.0662	3.55
4f9/2 - 4i9/2	3539.8	1.05e-20	1.01e-42	13.5	5.67	0.00440	52.1

Figure 8. The graphical user interface of LOMS online tool (<https://www.LOMS.cz>): Illustrative example of results structure for *Transition analysis*

334 Data Records

335 The complete set of blank template input files for each rare-earth ion, illustrative examples of input files together with attached
 336 results for JO and C-JO analysis and dataset of JO parameters listed in LOMS.cz database is available at Figshare³³ or the
 337 www.LOMS.cz webpage.

338 It presently, as of February 2025, contains:

- 339 1. **Template files:** complete set of eleven templates for Pr³⁺, Nd³⁺, Pm³⁺, Sm³⁺, Eu³⁺, Gd³⁺, Tb³⁺, Dy³⁺, Ho³⁺, Er³⁺ and
 340 Tm³⁺ trivalent rare-earth ions which contains: identification of $J \rightarrow J'$ transition with associated values of reduced matrix
 341 elements, mean-wavelengths and barycenters obtained from Walsh² JOFwin2011 documentation as a reference.
- 342 2. **Reference files:** example set of reference files with different types (I.–IV. of inputs, Fig.4) for JO analysis, C-JO analysis
 343 and calculation of radiative properties of Pr³⁺³⁴, Nd³⁺³⁵, Pm³⁺³⁶, Sm³⁺^{37,38}, Tb³⁺³⁹, Dy³⁺^{40,41}, Ho³⁺^{42,43}, Er³⁺^{31,44} and
 344 Tm³⁺^{45,46} trivalent rare-earth ions
- 345 3. **Combinatorial Judd-Ofelt analysis:** output files from C-JO analysis for RE³⁺-doped materials which contains JO
 346 parameters of all possible combinations of involved measured intrre- $4f$ transitions
- 347 4. **Database of Judd-Ofelt parameters:** more than 1200 data records of JO parameters and resulting radiative properties
 348 for 12 RE³⁺ ions in more than 550 materials/host matrices of various compositions

349 Structure of .csv file import

350 To standardize and simplify the data upload process, users can utilize the option to upload the required data via a .csv file,
 351 using the provided templates for all elements. The template .csv file for each RE³⁺ ion is unique and cannot be exchanged
 352 between each other since it contains the corresponding absorption transitions notation, assigned square matrix elements, etc. To
 353 successfully complete the form, the following steps must be completed:

- 354 1. **Template file:** Download the template file on the relevant rare-earth ion page (www.LOMS.cz/jo) or module documenta-
 355 tion (www.LOMS.cz/modules/judd-ofelt-analysis/) or from Figshare data repository³³
- 356 2. **Refractive index import:** Enter the refractive index input structure in the appropriate field following the *ref_index_type*
 357 cell (see Fig.9) as (1) *sellmeier* for input via Eq.21 or (2) *direct* for direct refractive index input. Based on your selection,
 358 enter either the Sellmeier coefficients or refractive index values for the corresponding transitions in the column labelled
 359 “refractive_index.”
- 360 3. **Transitions and Square matrix elements:** verify/replace the tabulated square matrix elements but do not change the
 361 labels of the individual transitions in the first column.
- 362 4. **Input type:** Select the corresponding form of your input type as follows: absorption cross section (*sigma*), experimental
 363 oscillator strength (*fext*), experimental linestrength (*sexp*) or JO parameters (*jo*) and write it down to the cell named
 364 *input_data* (rewrite it). The input values for corresponding transitions have to be placed in the same column. For the
 365 selection of JO parameters as an input (only for calculation of radiative properties), please insert the $\Omega_2, \Omega_4, \Omega_6$ JO
 366 parameters to the U^2, U^4, U^6 of the ground state (replace the zero values).
- 367 5. **Mean peak wavelength:** Enter the mean peak wavelengths for the transitions for which input data has been provided
 368 (see the previous text for proper estimation of mean wavelength value).
- 369 6. **Barycenter:** Check or provide relevant data for all transitions, otherwise it will not be possible to calculate the relevant
 370 radiation characteristics. Please see *Evaluation protocol and graphical software interface* section for more details
 371 regarding the proper barycenter selection.

LOMS Luminescence, optics and magneto-optics software
 Online tool for data fitting, simulation and evaluation

GRAPHICAL USER INTERFACE EXAMPLES
 Reference: 80TeO₂-20ZnO – 20BaO:Erx

Structure: Input file (template)

Please visit www.loms.cz for instructions how to fill this input file.

ref_index_type	sellmeier						
sellmeier_A	1						
sellmeier_B1	0						
sellmeier_C1	0						
sellmeier_B2	0						
sellmeier_C2	0						

Please visit www.loms.cz for instructions how to fill this input file.

excited_state	u2	u4	u6	input_data	mean_peak_wl_nm	refractive_index	barycenter
4I5/2	0	0	0	0	0		109
4I3/2	0.0194984	0.1173353	1.4316383	0	1520		6610
4I1/2	0.0281916	0.0003049	0.3952644	0	974		10219
4I9/2	0.1181329	0	0.0099097	0	801		12378
4F9/2	0	0.5353863	0.4617945	0	655		15245

Structure: Input file (reference, Er-doped material)

Reference data for Er - see www.loms.cz documentation for more details

ref_index_type	sellmeier						
sellmeier_A	1						
sellmeier_B1	2.63526						
sellmeier_C1	0.01608						
sellmeier_B2	0.32898						
sellmeier_C2	0.07885						

Data source: absorption cross section for calculation of JO2, JO4 and JO6 parameters and radiative properties Hrabovsky (2024)

excited_state	u2	u4	u6	sigma	mean_peak_wl_nm	refractive_index	barycenter
4I5/2	0	0	0	0	0		109
4I3/2	0.0194984	0.1173353	1.4316383	7E-19	1520		6570
4I1/2	0.0281916	0.0003049	0.3952644	9.41E-20	974		10202
4I9/2	0.1181329	0	0.0099097	3.41E-20	801		12412
4F9/2	0	0.5353863	0.4617945	1.48E-19	655		15247

Figure 9. The structure of import .csv file.

372 **Structure of .csv output file**

373 Calculated results of JO analysis, Combinatorial JO analysis and radiative transition properties can be exported in the form of
 374 .csv files upon clicking on the button *Export report* in the corresponding section (see Fig.6 and Fig.8). Example output files for
 375 the mentioned references are included in Figshare repository³³ and correspond to the data structures presented in Fig.6 and
 376 Fig.8. Data export from classical JO analysis also contains all input information for selected bands and both experimental and
 377 theoretical values of linestrength accompanied by the estimated ratios between calculated JO parameters.

Technical Validation: Judd-Ofelt analysis and Combinatorial Judd-Ofelt analysis

The general procedure of JO analysis, radiative transition analysis and C-JO analysis is shown in a flow chart in Fig.4 using four different input types: I. integrated cross section, II. experimental oscillator strength, III. experimental linestrength and IV. Judd-Ofelt parameters. Technical aspects and major steps in the process are described in the sections *Judd-Ofelt theory: Experimental practice* and *Evaluation protocol and graphical software interface*. The validity of the presented procedures is then presented in the following text on the examples of materials doped with Er^{3+} ^{31,44}, Dy^{3+} ^{40,41}, Ho^{3+} ^{42,43}, Nd^{3+} ³⁵, Pm^{3+} ³⁶, Pr^{3+} ³⁴, Sm^{3+} ^{37,38}, Tb^{3+} ³⁹ and Tm^{3+} ^{45,46} ions. Furthermore, C-JO analysis is provided for materials with more than four observed separate transitions, which allows the investigation of the most consistent and reliable outcomes using various combinations of absorption bands for JO analysis. Reference input files for all mentioned RE^{3+} -doped materials are included in Figshare data repository³³ together with a complete set of output files. The Combinatorial JO analysis results for selected RE^{3+} ions are presented within this text only in graphic form (Fig.10–13) due to the high number of possible combinations, where for 5, 6, 7, 8, 9, 10, 11, 12 and 13 experimentally observed input manifolds, it is possible to calculate 6, 22, 64, 163, 382, 848, 1816, 3797 and 8514 mutual manifolds combinations. Complete step-by-step procedure is presented here for the first reference of $\text{TeO}_2\text{--ZnO--BaO}$ tellurite glass doped with Er^{3+} ions (TZB:Er)³¹. Other references are presented in shorter form concerning calculated JO parameters and results of the Combinatorial JO analysis (see Table3).

The Er-doped material ($\text{TeO}_2\text{--ZnO--BaO}$ glass) was chosen as the main example due to the presence of a reasonable number (seven observed manifolds) of absorption bands across the optical transmission spectral window when some of them may overlap with each other. The visible part of the absorption spectrum of TZB:Er glass is shown in Fig.3. Derived dependency of baseline corrected absorption cross section was used to obtain the integral in Eq.18, which represents the integrated cross section (sum over the wavelength) for each observed manifold. These experimentally determined values were used as *Input type I* in the LOMS.cz software accompanied by the positions of mean wavelength and refractive index value for each manifold to calculate the experimental linestrengths values, which were used for JO fitting. Figshare data repository also contains other possible input types formats for this material, where *Input type II*: experimental oscillator strength, *Input type III*: experimental linestrength and *Input type IV*: JO parameters respectively. The last input type can be used together with known refractive index spectral dependency only for calculation of radiative properties. The placement of matrix elements (U^2 , U^4 , U^6), integrated cross section, mean wavelength and both experimental and theoretical linestrength values within LOMS.cz GUI interface is shown in Fig.5. The JO parameters were found to be $\Omega_2 = 7.66 \times 10^{-20} \text{cm}^2$, $\Omega_4 = 1.51 \times 10^{-20} \text{cm}^2$ and $\Omega_6 = 2.21 \times 10^{-20} \text{cm}^2$ which is in agreement with values presented in Ref.³¹ and values obtained by fitting procedure using the Walsh² evaluation software JOFwin(2011), where $\Omega_2 = 7.651 \times 10^{-20} \text{cm}^2$, $\Omega_4 = 1.508 \times 10^{-20} \text{cm}^2$ and $\Omega_6 = 2.208 \times 10^{-20} \text{cm}^2$. The JO parameters were then used to calculate the transition probabilities according to Eq.5 between any excited state and any lower-lying energy level and to calculate the branching ratios and radiative lifetimes. The obtained results are shown in Fig.8 and Table 2. Note, that the data structure in Table 2 is similar to the format of output file generated by LOMS online tool. The calculated values were again compared to those in Ref.³¹ and calculated using JOFwin2011² software with a good agreement. It is thus possible to verify the validity and accuracy of JO analysis fitting procedure and calculation of radiative properties. To further verify the validity of LOMS.cz software calculations, a similar procedure was applied to other materials doped with RE^{3+} ions using different data Input types and various number of observed manifolds. Calculated results are listed in Table3 with corresponding references and denoted number of used manifolds in the parentheses. The presented results are in good agreement with the associated reference values and possible deviations are caused by the use of different values of matrix elements, used constants and parameters or minor deviations in the calculation of linestrength values across the literature.

The reference datasets with more than four manifolds were used for providing C-JO analysis and investigation of results consistency as the function of involved absorption bands in the calculation of JO parameters. The Table 3 then contains the median values (Median) obtained from the set of all possible combinations and box-plot median values (Median BP)³¹ obtained from the statistically reduced set of possible combinations which can be compared to the values of JO parameters calculated using the maximum possible number of observed manifolds (Full.set). Graphical results of C-JO analysis are shown in Fig.(10–13). The complete output files are included in Figshare repository³³ for detailed inspections.

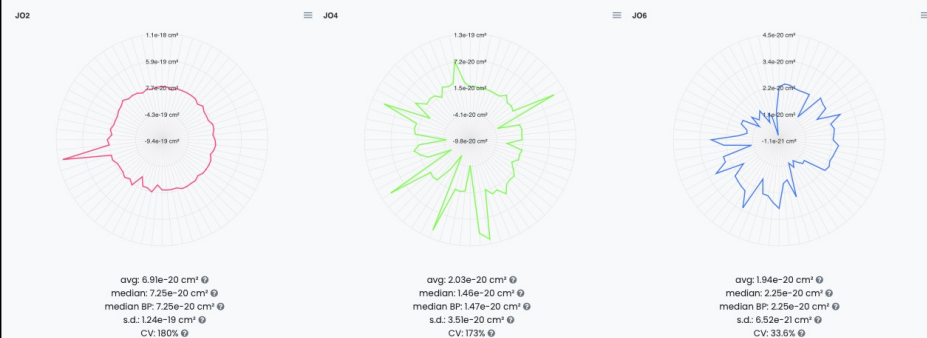
Table 2. Calculated Judd-Ofelt radiative transition properties in TZB:Er glass using LOMS.cz online tool (in similar format as the software output file). The Transition eState represent the initial excited state (J'), Transition gState represent the final ground/lower lying state (J), λ_{em} is the emission wavelength calculated as the difference between involved energy levels which positions is represented by insterted values of Barycenters, S(ED) and S(MD) are electric and magnetic dipole line strengths and their respective contributions to the electric and magnetic transition probabilities A(ED) and A(MD), β is the branching ration and last two columns represent the calculated values of radiative lifetime using the LOMS.cz online tool and those taken from Ref.³¹.

Transition eState	Transition gState	λ_{em} (nm)	S(ED)	S(MD) (cm ²)	A(ED) (s ⁻¹)	A(MD)	β	τ^{IO}_r (LOMS) (ms)	τ^{IO}_r (Ref. ³¹) (ms)
4I13/2	4I15/2	1547.7	3.49×10^{-20}	1.62×10^{-42}	388	78.3	1.00	2.14	2.15
4I11/2	4I15/2	990.8	1.09×10^{-20}	0.00	550	0.00	0.867	1.58	1.58
4I11/2	4I13/2	2753.3	2.91×10^{-20}	1.79×10^{-42}	66.5	17.7	0.133	11.9	11.9
4I9/2	4I15/2	812.8	2.84×10^{-21}	0.00	316	0.00	0.626	1.98	1.98
4I9/2	4I13/2	1711.7	1.60×10^{-20}	0.00	184	0.00	0.364	5.30	5.30
4I9/2	4I11/2	4524.9	4.06×10^{-21}	9.03×10^{-43}	2.50	2.42	0.00973	204	204
4F9/2	4I15/2	661.0	1.83×10^{-20}	0.00	3.90×10^3	0.00	0.895	0.229	0.230
4F9/2	4I13/2	1153.8	4.67×10^{-21}	0.00	177	0.00	0.0407	2.18	2.18
4F9/2	4I11/2	1986.1	3.39×10^{-20}	4.30×10^{-43}	249	13.7	0.0602	3.55	3.56
4F9/2	4I9/2	3539.8	1.05×10^{-20}	1.01×10^{-42}	13.5	5.67	0.00440	52.1	52.1
4S3/2	4I15/2	547.9	4.89×10^{-21}	0.00	4.77×10^3	0.00	0.683	0.143	0.144
4S3/2	4I13/2	848.2	7.65×10^{-21}	0.00	1.87×10^3	0.00	0.268	0.452	0.453
4S3/2	4I11/2	1225.9	1.70×10^{-21}	0.00	134	0.00	0.0192	2.92	2.92
4S3/2	4I9/2	1681.5	6.81×10^{-21}	0.00	206	0.00	0.0295	4.79	4.80
4S3/2	4F9/2	3203.1	5.88×10^{-22}	0.00	2.55	0.00	0.000366	392	392
2H11/2	4I15/2	526.3	6.29×10^{-20}	0.00	2.33×10^4	0.00	0.953	0.0408	0.0409
2H11/2	4I13/2	797.4	3.85×10^{-21}	3.26×10^{-43}	380	138	0.0212	0.873	0.874
2H11/2	4I11/2	1122.6	5.64×10^{-21}	1.17×10^{-43}	194	17.4	0.00864	1.59	1.60
2H11/2	4I9/2	1493.0	2.32×10^{-20}	2.19×10^{-44}	336	1.37	0.0138	2.41	2.41
2H11/2	4F9/2	2582.0	2.82×10^{-20}	2.54×10^{-44}	78.1	0.306	0.00320	12.7	12.8
2H11/2	4S3/2	13315.6	3.23×10^{-21}	0.00	0.0649	0.00	0.00000265	1.54×10^4	1.54×10^4
4F7/2	4I15/2	491.7	1.61×10^{-20}	0.00	1.12×10^4	0.00	0.838	0.0746	0.0747
4F7/2	4I13/2	720.6	5.09×10^{-21}	0.00	1.03×10^3	0.00	0.0772	0.461	0.462
4F7/2	4I11/2	976.0	7.62×10^{-21}	0.00	604	0.00	0.0450	0.883	0.884
4F7/2	4I9/2	1244.4	1.21×10^{-20}	1.61×10^{-43}	458	26.3	0.0361	1.89	1.89
4F7/2	4F9/2	1919.0	1.78×10^{-21}	5.46×10^{-43}	18.1	24.1	0.00315	22.0	22.0
4F7/2	4S3/2	4787.0	9.27×10^{-23}	0.00	0.0603	0.00	0.00000450	311	311
4F7/2	2H11/2	7473.8	1.85×10^{-20}	0.00	3.16	0.00	0.000236	316	317

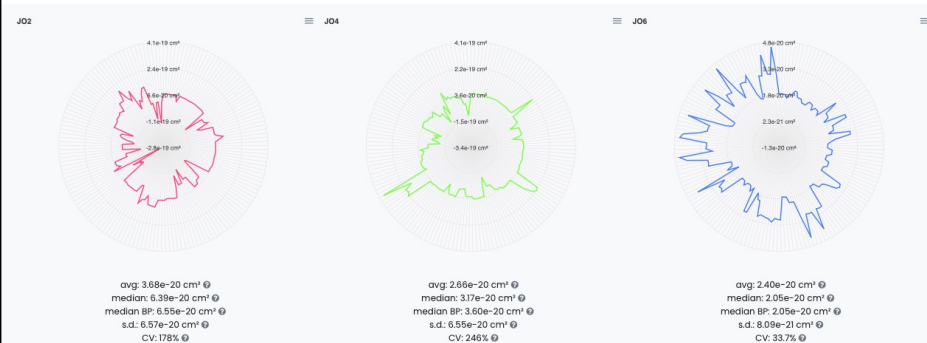
Table 3. Comparison of the Judd–Ofelt parameters Ω_i ($i = 2; 4; 6$) for various materials with denoted number of involved manifolds for JO analysis in parenthesis. Calculated JO parameters were obtained using all experimentally measured manifolds (Full.set) or as a median value from a complete set (Median) or reduced set (by Box plot method - Median BP) of possible combinations calculated using Combinatorial Judd-Ofelt analysis.

RE ³⁺	Host matrix	Involved transitions	Ω_2	Ω_4	Ω_6	Reference
			$(\times 10^{-20} \text{cm}^2)$			
Er ³⁺	80TeO ₂ –20ZnO–20BaO (glass)	Full.set (7)	7.66	1.51	2.21	Hrabovsky (2024) ³¹ and This work
		Median	7.25	1.46	2.25	
		Median BP	7.25	1.47	2.25	
	Ge ₂₅ -Ga _{9.5} Sb _{0.5} S ₆₅ (glass)	Full.set (4)	4.31	2.46	1.96	Strizik (2014) ⁴⁴ This work
		Full.set (4)	4.31	2.46	1.96	
		Full.set (8)	6.59	3.71	1.74	
Dy ³⁺	YVO ₄ (single crystal)	Full.set (8)	6.56	3.6	1.76	This work
		Median	6.39	3.17	2.05	
		Median BP	6.55	3.6	2.05	
	α -KGd(WO ₄) ₂	Full.set (13)	15.347	3.053	2.006	Kaminskii (2002) ⁴¹ This work
		Full.set (13)	15.7	2.72	2.12	
		Median	14.9	3.05	2.61	
	LiYF ₄ (single crystal)	Full.set (13)	1.03	2.32	1.93	Walsh (1998) ⁴³ This work
		Full.set (13)	1.03	2.31	1.94	
		Median	1.08	2.22	1.93	
	Y ₃ Al ₅ O ₁₂ (single crystal)	Full.set (12)	0.101	2.086	1.724	Walsh (2006) ⁴² This work
		Full.set (12)	0.102	2.08	1.73	
		Median	0.105	2.06	1.69	
	Y ₃ Al ₅ O ₁₂ (single crystal)	Median BP	0.171	2.06	1.69	
		Full.set (9)	3.1728	3.0819	1.9825	Walsh (2002) ³⁵ This work
		Full.set (9)	3.17	3.09	1.99	
Median	3.17	3.06	1.92			
Nd ³⁺	Y ₂ O ₃	Median BP	3.19	3.02	1.92	
		Full.set (7)	3.8	2.4	2.6	Shinn (1988) ³⁶ This work
		Full.set (7)	3.74	2.45	2.68	
Median	3.82	2.34	2.66			
Pm ³⁺	65PbO-20P ₂ O ₅ -6In ₂ O ₃ (glass)	Median BP	3.82	2.33	2.66	
		Full.set (7)	10.63	9.22	3.72	Merkle (2017) ³⁴ This work
		Full.set (7)	10.8	8.99	3.82	
Median	10.7	8.99	3.82			
Pr ³⁺	RbPb ₂ Cl ₅	Median BP	10.8	8.99	3.82	
		Full.set (13)	1.5	2.23	2.06	Vasyliiev (2013) ³⁹ This work
		Full.set (13)	1.51	2.23	2.06	
Median	1.07	2.69	1.67			
Tb ³⁺	LiTbF ₄	Median BP	1.52	2.46	1.68	
		Full.set (6)	0.52	0.284	0.398	Manjunath (2018) ³⁷ This work
		Full.set (6)	0.573	0.282	0.399	
Median	0.521	0.283	0.413			
Sm ³⁺	Sr ₂ SiO ₄	Median BP	0.521	0.293	0.413	
		Full.set (7)	0.48	2.04	1.83	Boudchica (2023) ³⁸ this work
		Full.set (7)	0.476	2.11	1.95	
Median	0.5	2.25	1.91			
	TeO ₂ BiCl ₃ (glass)	Median BP	0.964	2.29	1.89	
		Full.set (6)	6.14	1.54	0.87	Walsh (2006) ⁴⁵ This work
		Full.set (6)	6.22	1.49	1.22	
Median	6.37	1.57	1.22			
Tm ³⁺	GeO ₂ –BaO/CaO–Na ₂ O/Li ₂ O (glass)	Median BP	6.37	1.55	1.22	
		Full.set (4)	7.633	10.48	3.281	Bonner (2006) ⁴⁶ This work
		Full.set (4)	7.63	10.5	3.28	

TeO₂-ZnO-BaO:Er – 7 transitions, 64 possible combinations



YVO₄:Dy – 8 transitions, 163 possible combinations



alpha-KGd(WO₄)₂:Dy – 13 transitions, 8 514 possible combinations



Figure 10. Technical validation examples of combinatorial Judd-Ofelt analysis for materials doped with Er³⁺ and Dy³⁺ ions. Complete data outputs are listed in Figsahere repository³³

Y₃Al₅O₁₂:Ho (YAG:Ho) – 12 transitions, 3 797 possible combinations



LiF₄:Ho – 13 transitions, 8 514 possible combinations



Y₂O₃:Nd – 9 transitions, 382 possible combinations

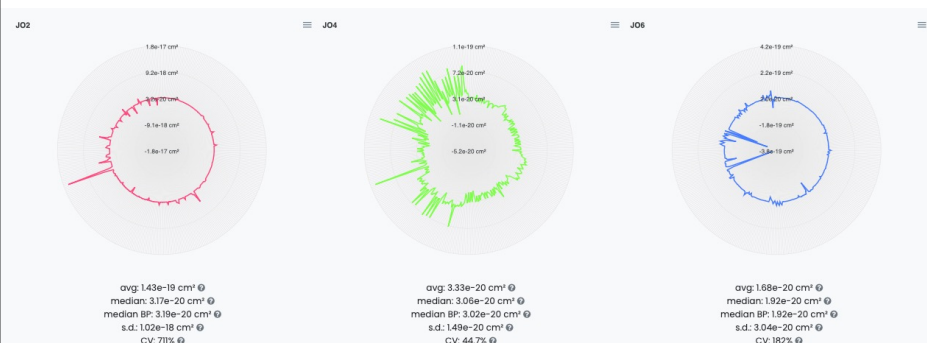
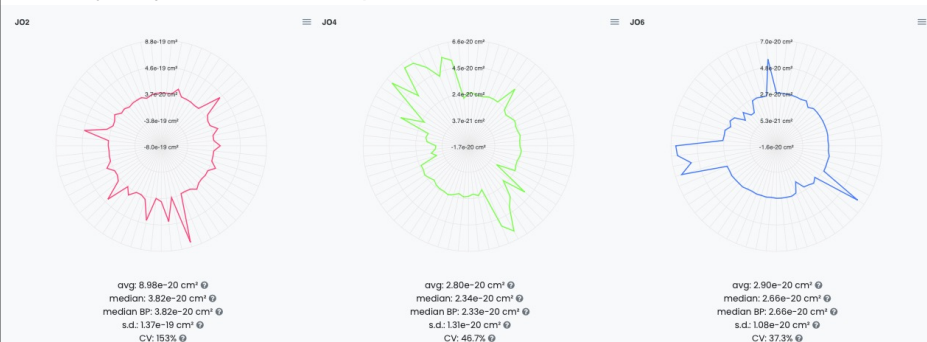


Figure 11. Technical validation examples of combinatorial Judd-Ofelt analysis for materials doped with Ho³⁺ and Nd³⁺ ions. Complete data outputs are listed in Figsahere repository³³

PbO–P₂O₅–In₂O₃:Pm – 7 transitions, 64 possible combinations



RbPb₂Cl₅:Pr – 7 transitions, 64 possible combinations

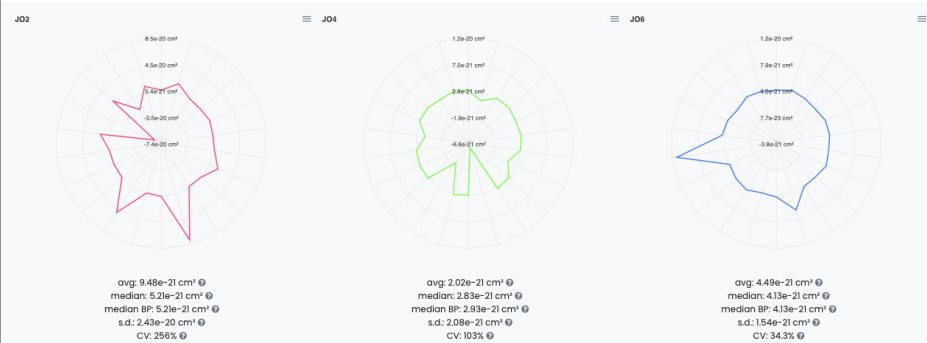


LiTbF₄ – 13 transitions, 8 514 possible combinations

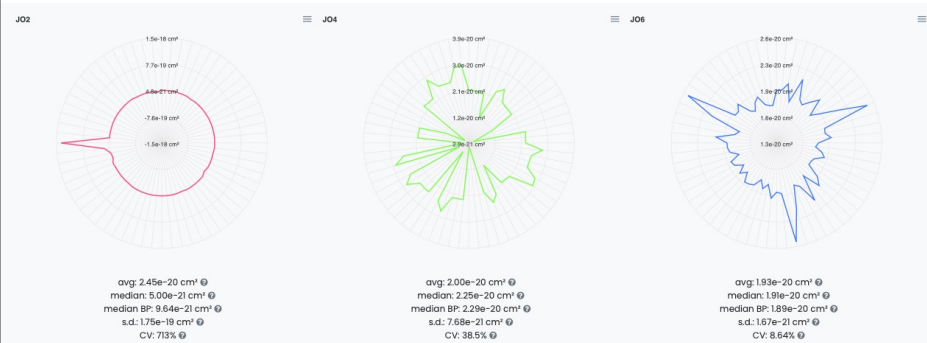


Figure 12. Technical validation examples of combinatorial Judd-Ofelt analysis for materials doped with Pm³⁺, Pr³⁺ and Tb³⁺ ions. Complete data outputs are listed in Figsahere repository³³

Sr₂SiO₄:Sm – 6 transitions, 22 possible combinations



TeO₂BiCl₃:Sm – 7 transitions, 64 possible combinations



Germanate glass: Tm – 6 transitions, 22 possible combinations

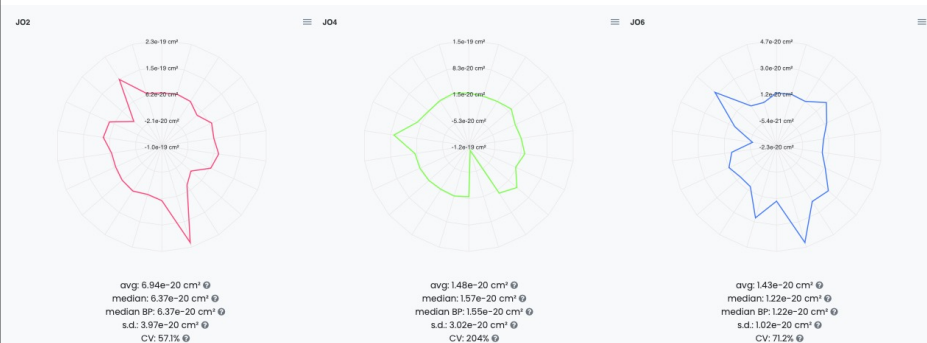


Figure 13. Technical validation examples of combinatorial Judd-Ofelt analysis for materials doped with Sm³⁺ and Tm³⁺ ions. Complete data outputs are listed in Figshare repository³³

423 Code availability

424 The complete set of blank template input files for each rare-earth ion, illustrative examples of input files together with attached
425 results for JO and C-JO analysis and dataset of JO parameters listed in LOMS.cz database is available at Figshare³³ or the
426 <https://www.LOMS.cz/> webpage.

427 The LOMS.cz Software is licensed for personal, classroom, education and internal use only and not for the benefit of
428 a third party (<https://www.LOMS.cz/about/>). The entire software codebase is publicly available on the LOMS.cz GitHub
429 project (<https://github.com/robinkrystufek/LOMS-JO>). Presented repository of JO parameters is regularly updated to meet
430 the ongoing scientific or industrial/engineering needs. Note that the data included in the JO parameters database and utilized
431 in template/reference files are sourced from publicly available, peer-reviewed publications, such as scientific journals and
432 handbooks/databooks. This curation ensures their reliability, and thus, their factual accuracy has not been further independently
433 verified. Every data entry in the dataset or/and reference/template file clearly references its source, allowing users to explore the
434 original data and its further context. The Luminescence, Optics, and Magneto-Optics software (www.LOMS.cz) thus stands
435 out as a vital resource by offering a user-friendly computational online tool for JO as well as C-JO analysis, and providing
436 a comprehensive database of JO parameters in a standardized file format. With regular updates and open access, it proves
437 indispensable for researchers, engineers, and students investigating the complex spectroscopic properties of rare-earth-doped
438 materials.

439 Conclusion

440 We have presented LOMS.cz, a comprehensive computational platform that addresses the long-standing challenge of standard-
441 izing Judd-Ofelt calculations in rare-earth spectroscopy. By integrating automated parameter computation, novel Combinatorial
442 JO analysis, and a dynamically expanding database of validated parameters, LOMS.cz enables reliable extraction of spec-
443 troscopic properties while providing rigorous uncertainty quantification. The platform's capabilities have been extensively
444 validated across diverse rare-earth systems including all spectroscopically active RE ions in various host matrices, demonstrating
445 excellent agreement with established literature values. Through its open-source nature and user-friendly interface, LOMS.cz es-
446 tablishes a foundation for accelerating the discovery and optimization of rare-earth-based photonic and optoelectronic materials.
447 The platform's modular architecture supports continued expansion of its capabilities through community contributions, while
448 its integrated database facilitates knowledge sharing and systematic comparison of results across different material systems. As
449 the field continues to evolve, LOMS.cz provides a standardized framework that will enable researchers to efficiently evaluate
450 materials properties and optimize rare-earth-doped systems for specific applications.

451 References

- 452 1. Wybourne, B. The fascination of the rare earths—then, now and in the future. *J. Alloy. Compd.* **380**, 96–100, [10.1016/j.
453 jallcom.2004.03.034](https://doi.org/10.1016/j.jallcom.2004.03.034) (2004).
- 454 2. Walsh, B. Judd-Ofelt theory: principles and practices. *Di Bartolo, B., Forte, O. (eds) Adv. Spectrosc. for Lasers Sens.*
455 https://doi.org/10.1007/1-4020-4789-4_21 (2006).
- 456 3. Zhou, B., Li, Z. & Chen, C. Global potential of rare earth resources and rare earth demand from clean technologies.
457 *Minerals* **7**, [10.3390/min7110203](https://doi.org/10.3390/min7110203) (2017).
- 458 4. Liu, G. & (eds), B. J. *Spectroscopic Properties of Rare Earths in Optical Materials* ((Springer 2005), 2005).
- 459 5. Zhou, B., Li, Z., Zhao, Y., Zhang, C. & Wei, Y. Rare earth elements supply vs. clean energy technologies: new problems to
460 be solve. *Gospodarka Surowcami Miner. - Miner. Resour. Manag.* **32**, [10.1515/gospo-2016-0039](https://doi.org/10.1515/gospo-2016-0039) (2016).
- 461 6. Gutfleisch, O. *et al.* Magnetic materials and devices for the 21st century: Stronger, lighter, and more energy efficient. *Adv.*
462 *Mater.* **23**, 821–842, [10.1002/adma.201002180](https://doi.org/10.1002/adma.201002180) (2011).
- 463 7. Sagawa, M., Fujimura, S., Togawa, N., Yamamoto, H. & Matsuura, Y. New material for permanent magnets on a base of
464 Nd and Fe (invited). *J. Appl. Phys.* **55**, 2083–2087, [10.1063/1.333572](https://doi.org/10.1063/1.333572) (1984).
- 465 8. Dong, H. *et al.* Lanthanide nanoparticles: From design toward bioimaging and therapy. *Chem. Rev.* **115**, 10725–10815,
466 [10.1021/acs.chemrev.5b00091](https://doi.org/10.1021/acs.chemrev.5b00091) (2015).
- 467 9. Zhou, J., Liu, Z. & Li, F. Upconversion nanophosphors for small-animal imaging. *Chem. Soc. Rev.* **41**, 1323–1349,
468 [10.1039/C1CS15187H](https://doi.org/10.1039/C1CS15187H) (2012).
- 469 10. HCSS/TNO. *Collaboration on Rare Earth Elements. An analysis of potentials for collaboration with Japan on Rare Earths*
470 (The Hague Centre for Strategic Studies and TNO: The Hague, Netherlands, 2012).

- 471 **11.** Tukker, A. Rare earth elements supply restrictions: Market failures, not scarcity, hamper their current use in high-tech
472 applications. *Environ. Sci. & Technol.* **48**, 9973–9974, [10.1021/es503548f](https://doi.org/10.1021/es503548f) (2014).
- 473 **12.** Hehlen, M., Brik, M. & Kramer, K. 50th anniversary of the Judd–Ofelt theory: An experimentalist’s view of the formalism
474 and its application. *J. Lumin.* **136**, 221–239, [10.1016/j.jlumin.2012.10.035](https://doi.org/10.1016/j.jlumin.2012.10.035) (2013).
- 475 **13.** Ciric, A., Marciniak, L. & Dramicanin, M. Self-referenced method for the Judd–Ofelt parametrisation of the Eu^{3+} excitation
476 spectrum. *Sci Rep* **12**, 563, [10.1038/s41598-021-04651-4](https://doi.org/10.1038/s41598-021-04651-4) (2022).
- 477 **14.** Judd, B. Optical absorption intensities of rare-earth ions. *Phys. Rev.* **127**, 750–761, [10.1103/PhysRev.127.750](https://doi.org/10.1103/PhysRev.127.750) (1962).
- 478 **15.** Ofelt, G. Intensities of Crystal Spectra of Rare-Earth Ions. *The J. Chem. Phys.* **37**, 511–520, <https://doi.org/10.1063/1.1701366> (1962).
- 479
- 480 **16.** Goldner, P. & Auzel, F. Application of standard and modified Judd–Ofelt theories to a praseodymium-doped fluorozirconate
481 glass. *J. Appl. Phys.* **79**, 7972–7977, [10.1063/1.362347](https://doi.org/10.1063/1.362347) (1996).
- 482 **17.** Smentek, L. *Judd-Ofelt Theory — The Golden (and the Only One) Theoretical Tool of f-Electron Spectroscopy*, chap. 10
483 (John Wiley Sons, Ltd, 2015).
- 484 **18.** Sytsma, J., Imbusch, G. & Blasse, G. The spectroscopy of Gd^{3+} in yttriumoxychloride: Judd–Ofelt parameters from
485 emission data. *J. Chem. Phys.* **91**, 1456–1461, [10.1063/1.457106](https://doi.org/10.1063/1.457106) (1989).
- 486 **19.** Görller-Walrand, C. & Binnemans, K. Chapter 167 spectral intensities of f-f transitions. In *Handbook on the Physics and*
487 *Chemistry of Rare Earths*, 101–264, [10.1016/S0168-1273\(98\)25006-9](https://doi.org/10.1016/S0168-1273(98)25006-9) (Elsevier, 1998).
- 488 **20.** Ciric, A., Stojadinovic, S. & Dramicanin, M. An extension of the judd-ofelt theory to the field of lanthanide thermometry.
489 *J. Lumin.* **216**, 116749, [10.1016/j.jlumin.2019.116749](https://doi.org/10.1016/j.jlumin.2019.116749) (2019).
- 490 **21.** Ciric, A., Stojadinovic, S. & Dramicanin, M. Approximate prediction of the cie coordinates of lanthanide-doped materials
491 from the judd-ofelt intensity parameters. *J. Lumin.* **213**, 395–400, [10.1016/j.jlumin.2019.05.052](https://doi.org/10.1016/j.jlumin.2019.05.052) (2019).
- 492 **22.** Hrabovský, J., Kučera, M., Paloušová, L., Bi, L. & Veis, M. Optical characterization of $\text{Y}_3\text{Al}_5\text{O}_{12}$ and $\text{Lu}_3\text{Al}_5\text{O}_{12}$ single
493 crystals. *Opt. Mater. Express* **11**, 1218–1223, [10.1364/OME.417670](https://doi.org/10.1364/OME.417670) (2021).
- 494 **23.** Hrabovský, J. *et al.* (preprint) rapid and precise large area mapping of rare-earth doping homogeneity in luminescent
495 materials. *Res. Sq.* [10.21203/rs.3.rs-4474095/v1](https://doi.org/10.21203/rs.3.rs-4474095/v1) (2024).
- 496 **24.** Lozykowski, H. Kinetics of luminescence of isoelectronic rare-earth ions in iii-v semiconductors. *Phys. Rev. B* **48**,
497 17758–17769, [10.1103/PhysRevB.48.17758](https://doi.org/10.1103/PhysRevB.48.17758) (1993).
- 498 **25.** Dieke, G. & Crosswhite, H. The spectra of the doubly and triply ionized rare earths. *Appl. Opt.* **2**, 675–686, [10.1364/AO.2.000675](https://doi.org/10.1364/AO.2.000675) (1963).
- 499
- 500 **26.** Peijzel, P., Meijerink, A., Wegh, R., Reid, M. & Burdick, G. A complete 4fn energy level diagram for all trivalent lanthanide
501 ions. *J. Sol. State Chem.* **178**, 448–453, [10.1016/j.jssc.2004.07.046](https://doi.org/10.1016/j.jssc.2004.07.046) (2005).
- 502 **27.** Vleck, J. The puzzle of rare-earth spectra in solids. *J. Phys. Chem.* **41**, 67–80, [10.1021/j150379a006](https://doi.org/10.1021/j150379a006) (1937).
- 503 **28.** Broer, L., Gorter, C. & Hoogschagen, J. On the intensities and the multipole character in the spectra of the rare earth ions.
504 *Physica* **11**, 231–250, [10.1016/S0031-8914\(45\)80009-5](https://doi.org/10.1016/S0031-8914(45)80009-5) (1945).
- 505 **29.** Edgar, A. *Optical properties of glasses*, in: *J. Singh (Ed.), Optical Properties of Condensed Matter and Applications* (John
506 Wiley Sons, 2006).
- 507 **30.** Wybourne, B. *Spectroscopic properties of Rare Earths* (Wiley (New York), 1965).
- 508 **31.** Hrabovsky, J. *et al.* Classical and combinatorial Judd–Ofelt analysis of spectroscopic properties in Er-doped materials:
509 $\text{TeO}_2\text{ZnOBaO}^{3+}$: glasses. *J. Phys. Photonics* **7**, 025006, [10.1088/2515-7647/adb115](https://doi.org/10.1088/2515-7647/adb115) (2025).
- 510 **32.** Polyanskiy, M. Refractiveindex.info database of optical constants. *Sci data* **11**, [10.1038/s41597-023-02898-2](https://doi.org/10.1038/s41597-023-02898-2) (2024).
- 511 **33.** Hrabovsky, J., Varak, P. & Krystufek, R. LOMS.cz: interactive online software for Classical and Combinatorial Judd-Ofelt
512 analysis with integrated database of Judd-Ofelt parameters. *Figshare* [10.6084/m9.figshare.c.7371784.v1](https://doi.org/10.6084/m9.figshare.c.7371784.v1) (2024).
- 513 **34.** Merkle, L. D. & Dubinskii, M. Pr:RbPb₂Cl₅: temperature dependent spectra, dynamics and three-for-one excitation. *Opt.*
514 *Express* **25**, 19780, [10.1364/OE.25.019780](https://doi.org/10.1364/OE.25.019780) (2017).
- 515 **35.** Walsh, B. M. *et al.* Spectroscopic characterization of Nd:Y₂O₃: application toward a differential absorption lidar system
516 for remote sensing of ozone. *J. Opt. Soc. Am. B* **19**, 2893, <https://doi.org/10.1364/JOSAB.19.002893> (2002).
- 517 **36.** Shinn, M. D., Krupke, W. F., Solarz, R. W. & Kirchoff, T. A. Spectroscopic and laser properties of Pm^{3+} . *IEEE J. Quantum*
518 *Electron.* **24**, 1100–1108, [10.1109/3.232](https://doi.org/10.1109/3.232) (1988).

- 519 **37.** Manjunath, C. *et al.* Optical absorption intensity analysis using judd-ofelt theory and photoluminescence investigation of
520 orange-red Sr_2SiO_4 : Sm^{3+} nanopigments. *Dye. Pigment.* **148**, 118–129, [10.1016/j.dyepig.2017.08.036](https://doi.org/10.1016/j.dyepig.2017.08.036) (2018).
- 521 **38.** Boudchicha, N. *et al.* Judd-Ofelt analysis and spectroscopy study of tellurite glasses doped with rare-earth (Nd^{3+} , Sm^{3+} ,
522 Dy^{3+} , and Er^{3+}). *Mater. (Basel)* **16**, 6832, [10.3390/ma16216832](https://doi.org/10.3390/ma16216832) (2023).
- 523 **39.** Vasyliov, V., Villora, E. G., Sugahara, Y. & Shimamura, K. Judd-Ofelt analysis and emission quantum efficiency of
524 Tb-fluoride single crystals: LiTbF_4 and $\text{Tb}_{0.81}\text{Ca}_{0.19}\text{F}_{42.81}$. *J. Appl. Phys.* **113**, 203508, [10.1063/1.4807649](https://doi.org/10.1063/1.4807649) (2013).
- 525 **40.** Cavalli, E., Bettinelli, M., Belletti, A. & Speghini, A. Optical spectra of yttrium phosphate and yttrium vanadate single
526 crystals activated with Dy^{3+} . *J. Alloy. Compd.* **341**, 107–110, [10.1016/S0925-8388\(02\)00079-8](https://doi.org/10.1016/S0925-8388(02)00079-8) (2002).
- 527 **41.** Kaminskii, A. *et al.* Optical spectroscopy and visible stimulated emission of Dy^{3+} ions in monoclinic α - $\text{KY}(\text{WO}_4)_2$ and
528 α - $\text{KGd}(\text{WO}_4)_2$ crystals. *Phys. Rev. B Condens. Matter* **65**, [10.1103/PhysRevB.65.125108](https://doi.org/10.1103/PhysRevB.65.125108) (2002).
- 529 **42.** Walsh, B., Grew, G. & Barnes, N. Energy levels and intensity parameters of ions in $\text{Y}_3\text{Al}_5\text{O}_{12}$ and $\text{Lu}_3\text{Al}_5\text{O}_{12}$. *J. Phys.*
530 *Chem. Solids* **67**, 1567–1582, [10.1016/j.jpcs.2006.01.123](https://doi.org/10.1016/j.jpcs.2006.01.123) (2006).
- 531 **43.** Walsh, B. M., Barnes, N. P. & Di Bartolo, B. Branching ratios, cross sections, and radiative lifetimes of rare earth ions in
532 solids: Application to Tm^{3+} and Ho^{3+} ions in LiYF_4 . *J. Appl. Phys.* **83**, 2772–2787, [10.1063/1.367037](https://doi.org/10.1063/1.367037) (1998).
- 533 **44.** Strizik, L. *et al.* Green, red and near-infrared photon up-conversion in Ga–Ge–Sb–S:Er³⁺ amorphous chalcogenides. *J.*
534 *Lumin.* **147**, 209–215, [10.1016/j.jlumin.2013.11.021](https://doi.org/10.1016/j.jlumin.2013.11.021) (2014).
- 535 **45.** Walsh, B. M., Barnes, N. P., Reichle, D. J. & Jiang, S. Optical properties of Tm^{3+} ions in alkali germanate glass. *J. Non*
536 *Cryst. Solids* **352**, 5344–5352, [10.1016/j.jnoncrysol.2006.08.029](https://doi.org/10.1016/j.jnoncrysol.2006.08.029) (2006).
- 537 **46.** Bonner, C. *et al.* A spectroscopic and Judd–Ofelt analysis of the relaxation dynamics of Tm^{3+} in the fluorapatites, FAP,
538 S-FAP, and B-FAP. *Opt. Mater. (Amst.)* **20**, 1–12, [10.1016/S0925-3467\(02\)00005-8](https://doi.org/10.1016/S0925-3467(02)00005-8) (2002).

539 Acknowledgements

540 This work was supported by the Charles University (SVV–2024–260720, GA UK No. 662220). This work was co-funded by
541 the European Union and the state budget of the Czech Republic under the project FERRMION CZ.02.01.01/00/22008/0004591.
542 This work was supported by the Czech Science Foundation, grants GA24-11361S and GA23-05507S. Petr Vařák acknowledges
543 the support of the junior grant awarded by the rector of UCT Prague. Besides that, authors would like to thank Lukas Strizik for
544 valuable comments and discussion. Special thanks belong to Brian M. Walsh for his long-lasting and significant contribution to
545 the field of RE ions spectroscopy and methodology of JO calculations which was an important factor in the development of this
546 work.

547 Author contributions statement

548 All authors contributed equally to this work. J.H.: conceptualization, methodology, software, validation, formal analysis,
549 investigation, visualization, supervision, funding acquisition and writing original draft, P.V. methodology, validation, formal
550 analysis, visualization, investigation and writing - Review and editing; R.K. methodology, software, validation, formal analysis,
551 visualization and writing - Review and editing. All authors reviewed the manuscript.

552 Competing interest

553 The authors declare no competing interests.

554 Additional information

555 Correspondence and request for materials should be addressed to J. Hrabovsky. Updated software documentation is available
556 at Luminescence, optics and magneto-optics software (LOMS) webpage <https://www.LOMS.cz/> as well as the GUI of the
557 software itself.